1 **Short running page heading:** Anatomy of archosaur lungs
2
3 **Title:** Anatomy, ontogeny, and evolution of the archosaurian respiratory system: a case study
4 on *Alligator mississippiensis* and *Struthio camelus*
5
6
7 **Author names and affiliations:**
8

9 Emma R. Schachner, [1]Brandon P. Hedrick, [2]Heather A. Richbourg, [3]John R. Hutchinson, [4]CG
10 Farmer
11
12 [*1]Department of Cell Biology & Anatomy, School of Medicine, Louisiana State University Health
13 Sciences Center, New Orleans 70112
14 [2]Department of Orthopaedic Surgery, University of California San Francisco, San Francisco,
15 California 94110
16 [3]Department of Comparative Biomechanical Studies, Royal Veterinary College, University of
17 London, Hatfield AL9 7TA, United Kingdom
18 [4]Department of Biology, University of Utah, Salt Lake City, UT 84102
19
20
21 **Corresponding author:**
22
23 Emma R. Schachner
24 Affiliation: Department of Cell Biology & Anatomy, School of Medicine, Louisiana State
25 University Health Sciences Center, New Orleans 70112
26 Email: eschachner@gmail.com
27

ABSTRACT

The avian lung is highly specialized and is both functionally and morphologically distinct from that of their closest extant relatives, the crocodilians. It is highly partitioned, with a unidirectionally ventilated and immobilized gas-exchanging lung, and functionally decoupled, compliant, poorly vascularized ventilatory air-sacs. To understand the evolutionary history of the archosaurian respiratory system, it is essential to determine which anatomical characteristics are shared between birds and crocodilians and the role these shared traits play in their respective respiratory biology. To begin to address this larger question, we examined the anatomy of the lung and bronchial tree of ten American alligators (*Alligator mississippiensis*) and eleven ostriches (*Struthio camelus*) across an ontogenetic series using traditional and micro-computed tomography (µCT), three-dimensional (3D) digital models, and morphometry. Intraspecific variation and left to right asymmetry were present in certain aspects of the bronchial tree of both taxa but was particularly evident in the cardiac (medial) region of the lungs of alligators and the caudal aspect of the bronchial tree in both species. The cross-sectional area of the primary bronchus at the level of the major secondary airways and cross-sectional area of ostia scaled either isometrically or negatively allometrically in alligators and isometrically or positively allometrically in ostriches with respect to body mass. Of fifteen lung metrics, five were significantly different between the alligator and ostrich, suggesting that these aspects of the lung are more interspecifically plastic in archosaurs. One metric, the distances between the carina and each of the major secondary airways, had minimal intraspecific or ontogenetic variation in both alligators and ostriches, and thus may be a conserved trait in both taxa. In contrast to previous descriptions, the 3D digital models and CT scan data demonstrate that the pulmonary diverticula pneumatize the axial skeleton of the ostrich directly from the gas-exchanging pulmonary tissues instead of the air sacs. Global and specific comparisons between the bronchial topography of the alligator and ostrich reveal multiple possible homologies, suggesting that certain structural aspects of the bronchial tree are likely conserved across Archosauria, and may have been present in the ancestral archosaurian lung.

KEY WORDS: Aves, Crocodylia, Lungs, Pulmonary, Computed Tomography, 3D modeling

INTRODUCTION

The lung has evolved a structural diversity (Fig. 1) that has confounded comparative biologists for centuries despite a common function as the primary site of gas exchange in the majority of vertebrates (Farmer, 2006, Farmer, 2010, Huxley, 1882, Maina, 2017, Sappey, 1847). Particularly enigmatic is the origin of the highly specialized avian respiratory system, with its functionally decoupled, unidirectionally ventilated immobile gas-exchanging lung (i.e., air travels in the same direction through most of the bronchial tree during both inspiration and expiration), and flexible, poorly vascularized air sacs (Maina, 2017). The microscopic and macroscopic anatomy of the avian respiratory system has been well documented through gross dissection, latex casts, and scanning electron microscopy (Duncker, 1971, Duncker, 1972, King, 1966, Maina, 2007, Maina, 1989, Maina, 2006a, O'Connor, 2004). However, the complete three-dimensional (3D) anatomy has been difficult to study *in situ* prior to the introduction of computed tomographic (CT) and microCT (µCT) methodologies. This has resulted in an incomplete understanding of many aspects of lung morphology, including the relationships between the bronchial tree and the air sac system, degree of intra- and interspecific variation

74 and ontogenetic changes, and relationships between the respiratory system and the adjacent
75 skeletal tissues. Additionally, despite over a century of study on airflow patterns in the avian
76 lung, the mechanisms by which unidirectional flow is maintained within the bronchial tree
77 remains elusive (Harvey and Ben-Tal, 2016, Maina, 2017, Maina and Africa, 2000, Maina et al.,
78 2009).
79   To begin to disentangle the origins of the complex avian respiratory system, it is
80 essential to understand the respiratory system of their only extant archosaurian relatives, the
81 crocodilians. The pulmonary anatomy and respiratory function of crocodilians has received
82 considerably less attention than their avian counterparts; however, the recent discovery of
83 unidirectional airflow patterns in the lungs of numerous species of crocodilians (Farmer, 2010,
84 Farmer, 2015b, Farmer and Sanders, 2010, Schachner et al., 2013), a monitor lizard (Cieri and
85 Farmer, 2019, Schachner et al., 2014), and the green iguana (Cieri et al., 2014), suggest that the
86 origin of unidirectional airflow predates the evolution of avian flight, and is likely independent
87 from the evolution of birds and endothermy (Cieri et al., 2014, Cieri and Farmer, 2016,
88 Schachner et al., 2014). Recent work in gross anatomy, embryonic development, function, and
89 in vascularization patterns has demonstrated potential homologies between the crocodilian
90 and avian lung (Farmer and Sanders, 2010, Sanders and Farmer, 2012, Schachner et al., 2013,
91 Farmer, 2015b).
92   To investigate the functional biology and evolutionary history of the avian and
93 crocodilian respiratory systems, we first determine which morphological traits are shared
94 between the extant members of both groups (i.e., phylogenetic bracketing following Witmer,
95 1995) through a series of qualitative and quantitative comparisons. We present the detailed
96 gross anatomy and variation in the bronchial tree of the American alligator (*Alligator*
97 *mississippiensis*; n = 10) and the ostrich (*S. camelus*; n = 11) using 3D digital models generated
98 via traditional CT and μCT across an ontogenetic series. In both taxa, comparative
99 measurements were taken between anatomically relevant characteristics of the large primary
100 and secondary branches of the bronchial tree that are hypothesized to be associated with
101 unidirectional airflow based upon previously published studies (Brackenbury, 1972, Butler et al.,
102 1988, Duncker, 1971, Farmer, 2015b, Farmer and Sanders, 2010, Maina and Nathaniel, 2001,
103 Maina, 2006a, Sanders and Farmer, 2012, Schachner et al., 2013), using hypotheses of
104 homology derived from Broman (1939), Sanders and Farmer (2012), and Schachner et al.
105 (2013). These data are used to (1) establish intra- and interspecific variation in archosaurian
106 lung morphology, (2) assess hypotheses of homology between the avian and crocodilian
107 respiratory systems, and (3) provide comparative data useful in reconstructing the ancestral
108 archosaurian bronchial tree. This initial dataset will be critical for future comparisons with other
109 avian taxa occupying different ecological and functional niches, and the other less well studied
110 crocodilian taxa. These data will also be integral for the generation of hypothesis of homology
111 for developmental studies on the pulmonary architecture in archosaurs.
112
113 **MATERIALS AND METHODS**
114
115 **Computed tomography and specimens**
116   CT scans were obtained from ten specimens of American alligator (*A. mississippiensis*),
117 and eleven ostriches (*S. camelus*) (see Table 1 for the information on the specimens used in this
118 study). The alligators were obtained from the Louisiana Department of Wildlife and Fisheries at
119 the Rockefeller Wildlife Refuge; deceased animals were collected for purposes unrelated to this

120   study. Scans of the live *A. mississippiensis* were also conducted for an unrelated study, but
121   followed the IACUC guidelines of the University of Utah. Five scans were performed on lungs
122   stained with potassium iodide (I_2KI) (Jeffery et al., 2011) (four *A. mississippiensis* and one *S.*
123   *camelus*). The *S. camelus* specimens were obtained from the OK Corral Ostrich Farm in
124   Southern California and acquisitioned into the collections of the University of California
125   Museum of Vertebrate Zoology (MVZ) and the Royal Veterinary College, London. The juvenile
126   ostriches died of natural causes and were donated to the MVZ for research purposes. With the
127   exception of the alligator hatchling and the adult ostrich, all animals were scanned at either the
128   University of Utah Medical Center, Research Park, or the South Jordan Medical Center on a 164
129   slice dual energy Siemens SOMATOM Definition computed tomography unit. Image acquisition
130   parameters included: slice thickness 0.6–1 mm, 120 kVp, 200–400 MA (Table 1). The data were
131   filtered in soft tissue and lung algorithm and edge-enhanced with a high-resolution lung
132   algorithm. The CT data from the alligators and ostriches are available via Data Dryad (DOI:
133   https://doi.org/10.5061/dryad.3xsj3txdh).
134
135   **Anatomical digital modeling, quantitative measures, and analysis**
136   The pulmonary bronchi, lung surface, and skeleton (Fig. 2) were segmented into a three-
137   dimensional (3D) surface mesh model with the visualization software Avizo 7.1 (FEI
138   Visualization Sciences Group). Measurements of airway dimensions were taken in OsiriX MD -
139   OsiriX DICOM Viewer (www.osirix-viewer.com) and are included in the Supplemental
140   Information (SI Table 1, 2). These measurements were chosen based upon hypothesized
141   homologous structures in both taxa (Table 2) from previous anatomical (Sanders and Farmer,
142   2012, Schachner et al., 2013) and developmental studies (Broman, 1939, Locy and Larsell,
143   1916a, Locy and Larsell, 1916b). Qualitative anatomical similarities observed between the large
144   secondary airways in the adult and embryonic crocodilian and avian bronchial trees, and
145   functional similarities in airflow patterns previously described through experimental work were
146   used to inform metrics selected for the quantitative component of this analysis (Brackenbury,
147   1979, Butler et al., 1988, Duncker, 1971, Farmer, 2015b, Farmer, 2015a, Schachner et al., 2013).
148   To assess the lungs quantitatively, the following metrics were collected and are
149   illustrated in Fig. 3: (1) maximum diameter and area of the trachea proximal to the bifurcation
150   (2) maximum diameter and area of the right extrapulmonary primary bronchus just distal to the
151   bifurcation off of the trachea; (3) area of the primary bronchus just proximal to the opening of
152   the ostium of the major secondary airways arising off of the primary bronchus: the cervical
153   ventral bronchus (CVB) in the alligator and ventrobronchus (V) 1 in the ostrich, and the first
154   four dorsobronchi in both taxa (D2-D5 in the alligator, D1-4 in the ostrich); (4) area of the
155   ostium of each of the secondary airways in both taxa (the CVB and D2-5 in the alligator, V1 and
156   D1-4 in the ostrich); (5) area of the ostium of the first two clearly observable laterobronchi in
157   both taxa; and, (6) distance from the carina to the center point of each of the ostia for each of
158   the major secondary airways: CVB, D2-5 (alligator); V1-4, D1-4 (ostrich). To measure the ostium
159   of each bronchus as accurately as possible, the DICOMs were rotated and re-sliced in the OsiriX
160   3D MPR Viewer window so that each of the three windows was properly aligned with the
161   ostium or bronchus being measured. Specifically: (1) one viewer was oriented to show the
162   opening of the ostium as close to the primary bronchus as possible; (2) the second viewer was
163   rotated so that it sliced through, and aligned with the middle of the primary bronchus; and, (3)
164   the third viewer was oriented so that it aligned with the orientation of the bronchus itself. Since
165   all of the airways are organic structures, and thus curve and branch, each of the windows had

166 to be adjusted for the measures completed at each site listed above. All measures were
167 completed by E.R. Schachner to eliminate inter-observer error in the 3D MPR viewer of OsiriX.
168 To minimize intra-observer error, each measurement was completed three times, and then
169 averaged. To validate the measurements completed in OsiriX, an object of known dimensions
170 was scanned with the hatchling alligator and was measured.
171

Body mass and interspecific comparisons
173 Age at time of death was unknown for the majority of specimens. Therefore, scaling and
174 comparisons between species were based on body masses only. It is well established that body
175 mass can vary due to environmental factors aside from age, particularly in crocodilians (e.g.,
176 temperature or food consumption) (Saalfeld et al., 2008), so comparisons based on absolute
177 age are outside of the scope of this study. Body mass was not available for four of the ten
178 alligators, so mass was estimated using the Multivariate Imputation by Chained Equations
179 (MICE) package (van Buuren and Groothuis-Oudshoorn, 2011) in R (R Core Development Team,
180 2018, version 3.5.2), which imputes missing data points based on a value drawn from a
181 distribution created from other variables from the dataset. We identified two measures that
182 strongly and significantly correlated with the known masses in all six alligators: right primary
183 bronchus maximum diameter and right primary bronchus area (Fig. 4). These measures and the
184 mass (if known) were input and a series of 100 iterations were completed to estimate missing
185 masses (SI Table 3). The final mass for each specimen for analysis was the mean of the 100
186 imputed values for that individual. These include: *A. mississippiensis* 54 mass: mean 10kg (95%
187 Confidence Interval (CI) of $\pm$1.563); *A. mississippiensis* "Stumpy" mass: mean 13.4kg (95% CI of
188 $\pm$2.427); *A. mississippiensis* 64 mass: mean 14.5kg (95% CI of $\pm$1.987); and *A. mississippiensis* 81
189 mass: mean 31.5kg (95% CI of $\pm$6.628).
190 Prior to the analyses, all values were log10 transformed. Fifteen model II standard major
191 axis (SMA) regressions were run between lung metrics and body mass using the lmodel2
192 package in R (Legendre, 2018) to assess allometric intraspecific trends. SMA regressions are
193 preferred over ordinary least squares regressions when both variables (lung variables and body
194 mass) are subject to measurement error (Sokal and Rohlf, 2012). Confidence intervals ($\alpha = 0.05$)
195 were calculated around slopes to evaluate deviations from isometry. Differences between the
196 alligator and ostrich trajectories were then statistically compared using SMA confidence
197 intervals of the slopes and y-intercepts. Additionally, relative differences in distances from the
198 carina to the secondary bronchi (CVB, D2, D3, D4, D5) were visualized as percentages of total
199 distance (from the carina to D5) in each *A. mississippiensis* and *S.camelus* specimen to assess
200 relative variation in distances both intra- and interspecifically.
201

Caveats
203 The lungs of one ostrich and four of the alligators were stained with I_2KI to make the
204 parenchyma more visible in these specimens. It has been well established that this
205 methodology causes some shrinkage in the tissues (Gignac et al., 2016), and can cause dramatic
206 shrinkage when specimens are stained for substantial lengths of time, e.g., weeks (Hedrick et
207 al., 2018). None of these specimens were fixed prior to staining or stained for longer than 24
208 hours which are significant contributors to tissue deformation (Gignac et al., 2016, Hedrick et
209 al., 2018). Additionally, the majority of the quantitative metrics obtained from the bronchial
210 tree in the alligators were collected from the proximal portion which is cartilaginous in nature

211 (CVB, L, D2–3 and associated PB measures) and the avian bronchial tree is immobilized and thus
212 less flexible than other pulmonary tissues (e.g., Maina, 2006b, Maina, 2017).
213
214 **RESULTS**
215
216 **Anatomy of the bronchial tree in *Alligator mississippiensis***
217 We examined *Alligator* lung morphology (Sanders and Farmer, 2012) based on a large
218 intraspecific sample including various ontogenetic stages (Figs. 5-8) to build on previous work
219 done by Sanders and Farmer (2012) and Schachner et al. (2013) (Table 2). Terminology for the
220 bronchi was based on that used for the developing lung (Broman, 1939).
221 **Primary bronchus** Just distal to the carina, the cartilaginous portion of the primary
222 bronchi extends caudally just past the cone-shaped ostium of the cervical ventral bronchus.
223 Distal to the end of the cartilaginous portion, the primary bronchus expands into a hook-shaped
224 bronchus (round to sub-elliptical in cross section) that curves medially, terminating in a small
225 tapered point (Figs. 5-8). A variable number of small to medium-sized balloon-shaped bronchi
226 emerge off of the caudal margin of the primary bronchus (Figs. 6; 8A, D, J). There is a
227 considerable amount of bilateral asymmetry in the overall morphology of the caudal portion of
228 the primary bronchi in *A. mississippiensis*, and a grossly visible differential distribution of the
229 respiratory parenchyma, with the majority of the parenchyma occupying the dorsal region of
230 the lung (Fig. 7G, H).
231 **Cervical ventral bronchus (CVB)** In *A. mississippiensis*, the first bronchus to branch off of
232 the intrapulmonary primary bronchus is the CVB. It originates from a robust cartilaginous cone
233 that makes a hairpin turn immediately after branching off of the primary bronchus so that the
234 orientation of the long axis of the bronchus lies almost parallel with the trachea (Figs. 5A-D; 6).
235 There is significant variability in the appearance of the CVB between different alligators (Fig. 8).
236 This appears to be due to intraspecific variation in overall structure, as well as other
237 parameters, including the level of lung inflation, how full the stomach of the animal is, and
238 whether or not the lung was inflated inside or outside of the body. In all alligators, the CVB is
239 accompanied by multiple tertiary bronchi that run ventrally and then cranially in tandem with
240 the main CVB bronchus (Figs. 6A, 8). The majority of these tertiary bronchi arise from either the
241 cartilaginous CVB cone, or the proximal two thirds of the CVB itself. The number, size, and
242 morphology of the tertiary bronchi are one of the most variable characters in the alligator lung
243 but tend to be similar between the left and right lungs (with the exception of one individual
244 where the CVB forked distally on one side).
245 **Dorsobronchi (D2–5)** The dorsobronchi arise sequentially along the dorsal surface of the
246 primary bronchus caudal to the cone-shaped ostium of the CVB (Figs. 5A-D; 6A; 7). These
247 bronchi diminish in size (overall length and bronchial diameter) as they continue caudally. There
248 are typically four on either lung, but a small fifth dorsobronchus has been identified on the right
249 lung of one individual (alligator 9). The dorsobronchi arise from large oval-shaped ostia (Fig.
250 6A), arch dorsally, and then travel cranially, tapering out to a small pointed tip (Fig. 8A, C, D, F,
251 G, I, J, L). The first dorsobronchus (D2) travels to the apex of the lung usually connecting with
252 the distal tip of the CVB via a parabronchus (Fig. 7B). There are multiple tube-like connections
253 (i.e., structures hypothesized to be homologous with the avian parabronchi (Schachner et al.,
254 2013) linking the dorsobronchi with both the CVB, and one another, along their length (Fig. 7B).
255 The caudal-most dorsobronchus (D5) tends to be very small, often not extending cranially at all.

256   Tertiary bronchi predominantly arise from the base of each dorsobronchus with the exception
257   of some larger tube-shaped bronchi that originate on the lateral surface of D2 (Fig. 5D).
258   **Medial bronchi (M1–5)** There is considerable variation in the morphology and number
259   of medial bronchi, with the degree of morphological variation increasing caudally. All alligators
260   examined possessed paired M1 bronchi that were consistently the second branch to arise off of
261   the primary bronchus and serve as the source for the first (or cranial-most) bronchus of the
262   cardiac lobe. M1 arises medially, arches slightly dorsally and then runs cranially for its entire
263   length often in unison with D2 (Figs. 5E; 6). Only M1 is bilaterally symmetric. M2 and M3 on the
264   left lung arise medially and tend to rise dorsally often giving off both cranial and caudal
265   branches (Figs. 5E; 6). In the right lung, these same bronchi frequently extend medially and
266   caudally. In most of the individuals examined, there were more medial bronchi on the right lung
267   than the left; however, in one specimen (alligator 64), there were 5 medial bronchi on the left
268   lung, and three on the right. The more caudal medial bronchi give rise to the second and third
269   branches (if present) of the cardiac lobes. In a few specimens, the caudal bronchi of the cardiac
270   lobes branch directly off of the medial surface of the primary bronchus.
271   **Laterobronchi (L)** The laterobronchi are sac-like, poorly vascularized bronchi that
272   originate from small ostia along the lateral and ventral surfaces of the primary bronchus
273   beginning slightly distal to the cartilaginous cone of the CVB (Figs. 5F; 6). The anatomy of the
274   laterobronchi varies between both right and left lungs and between individuals. However, there
275   is an overall morphological trend in that these bronchi conform to a narrow, constricted origin
276   that balloons out into a multi-fingered, sac-like distal end, which expands in all directions.
277   These bronchi occupy the distensible caudoventral floor of the lung and come in contact with
278   the liver when *in situ*.
279   **Caudal group bronchi (CGB)** There are numerous tube-shaped bronchi that arise
280   predominantly from the ventral surface of the primary bronchus caudal to the laterobronchi
281   (although some small CGB arise from the dorsal surface of the primary bronchus) (Figs. 5F; 7).
282   Like the laterobronchi, these secondary branches occupy the flexible caudoventral floor of the
283   lung and are in contact with both the cranial surface of the liver and stomach. The ostia of the
284   CGB are much larger than those of the laterobronchi, and the transition between the two types
285   of bronchi is evident by both gross dissection and CT. These bronchi can also be differentiated
286   from the laterobronchi in their honeycomb shape versus the finger-like sac shape of the
287   laterobronchi. They are, however, similar in that they are grossly dead-end structures –
288   although there may be small inter-bronchial perforations that are not visible via dissection or
289   medical grade CT. There is some individual variation in the overall morphology of the CGB. In
290   some specimens, they are small, or sparse (alligators 81 and 11); however, in others, they are
291   much larger in size (alligator 64 and hatchling alligator AM041315-1) (Figs. 5, 7). No obvious
292   relationship was evident between the number and size of the CGB and the state of the lungs, or
293   specimen size.
294   **Cardiac lobes (C1–4)** There are a collection of secondary and tertiary bronchi that, due
295   to their arrangement and position, make up the cardiac lobes. These bronchi branch off of the
296   medial bronchi, or medial aspect of the primary bronchus in a variable manner. The lobes,
297   which contain expanded individual bronchi, arise asymmetrically off of both lungs with the
298   primary lobe (the lobe with the largest cranial-most bronchus that occupied the space in
299   between the primary bronchi and the carina) emerging from the right lung in all examined
300   individuals (Figs. 5F; 6B; 7E, F; 8B, E, H, K). The number of bronchi that contribute to the cardiac
301   lobes and actual size of each lobe was variable (Table 3). For example, there was one bronchus

302 in the left lung and two in the right in one individual (*A. mississippiensis* 11), three on each side
303 in three individuals (alligators 739, 15, 12), and four bronchi contributing to the left lobe and
304 two to the right in another (alligator 64). There was no clear relationship between number of
305 bronchi in the cardiac lobes, size of the animal, level of lung inflation, or state of the lungs (i.e.,
306 in a live animal or excised).
307
308 **Anatomy of the bronchial tree in *Struthio camelus***
309   Recent work has made substantial strides in addressing the confusion surrounding the
310 anatomy of the bronchial tree in *S. camelus* using digital models (Maina and Nathaniel, 2001,
311 Maina et al., 2009), but these models do not show the entire bronchial tree and air sacs in
312 detail, or as an intact organ system *in situ*. Therefore, we present a complete and detailed
313 model of the lower respiratory system of *S. camelus* (Figs. 9-16) and explore the relationship
314 between the respiratory system and the post-cranial skeleton (Figs. 13, 15).
315   **Primary bronchi** The cartilaginous primary bronchi are short and slightly constricted just
316 distal to the carina. Distal to the hilus, the primary bronchi are round to sub-elliptical in cross
317 section and increase in diameter, until approximately the origin of the third dorsobronchus
318 (Figs. 10D, 11). They then taper caudally (approximately 1/3 the maximum diameter) continuing
319 to, and beyond the caudal margin of the gas-exchanging region of the lung, where they expand
320 and balloon into the abdominal air sac. In lateral view, the primary bronchi have a low
321 horizontal arc (Figs. 10D, 11).
322   **Ventrobronchi (V1–4/5)** There are variably four to five ventrobronchi in the ostrich,
323 which arise sequentially off of the dorsomedial surface of the primary bronchus immediately
324 distal to the hilus (Figs. 10C; 11A, C). The ventrobronchi arise in close proximity with only a thin
325 (0.32–0.88 mm) septum of the primary bronchus separating them. The first ventrobronchus
326 (V1) is the largest and most well developed, sending large tertiary branches cranioventrally,
327 which loop around the cranial aspect of the primary bronchus, and caudomedially, which give
328 off smaller quaternary branches that run medially (Figs. 10C; 11A, C; 12E). At its distal tip, the
329 craniomedial branch of V1 enlarges into the cervical air sac. The more dorsomedially oriented
330 bronchi emanating from V1 unite with their equivalent from the other lung and expand into the
331 cervical air sac. V1 has the highest number of large tertiary and quaternary branches relative to
332 the more caudal ventrobronchi. The second ventrobronchus (V2) arises just caudally to V1 from
333 a slightly more medially oriented ostium (Figs. 10C; 11A, C). V2 immediately bifurcates, sending
334 a single branch laterally over the primary bronchus to run ventrally, expanding distally into the
335 cranial thoracic air sac. The medial branch of V2 runs caudomedially along the ventral surface of
336 the gas-exchanging lung, sending off variably sized smaller bronchi. The third ventrobronchus
337 (V3) originates just caudal to the ostium of V2 and mirrors the caudomedial aspect of V2 (Fig.
338 10C). V3 has a slightly larger diameter throughout its length relative to V2 in all of the ostriches
339 examined; it also sends off a variable number of smaller branches that all project caudally. The
340 fourth (and usually last) ventrobronchus (V4) emerges from the primary bronchus just caudal to
341 the ostium of V3. It is approximately half the length of V3 and is much smaller in diameter.
342 There are generally few or zero visible large-diameter tertiary bronchi arising from V4 (Fig.
343 10C). In two of the eleven ostriches examined, there is a fifth ventrobronchus (V5), which
344 morphologically resembles V4, but is much smaller in length and diameter.
345   **Dorsobronchi** There are a variable number of dorsobronchi in *S. camelus,* ranging from
346 8–11 that are visible via CT (Figs. 10D; 11A, C; 12E). There is some bilateral asymmetry in the
347 dorsobronchi, but this may be due to associated problems derived from tissue decay rather

348 than true biological asymmetry. In light of this, only the first four dorsobronchi will be described
349 in detail, with the remaining branches described as a unit. All of the dorsobronchi arise
350 sequentially (like the ventrobronchi) with minimal space between ostia (Figs. 10D; 11A, C). The
351 ostia are slightly offset dorsally relative to the more medial origins of the ventrobronchi, and in
352 most of the individuals examined, there is a small diastema (cranial to caudal) between the last
353 ventrobronchus and the first dorsobronchus (Fig. 11A, C). Dorsobronchus 1 (D1) has an elliptical
354 shaped ostium, and arcs craniodorsally, giving off a variable number of tertiary bronchi that run
355 cranially and ventrally (Fig. 10E). The second dorsobronchus (D2) is the largest (both in
356 bronchial width and the development of the tertiary and quaternary branches; Fig. 10D). It is
357 fan-shaped and runs dorsally at its base, with its tertiary branches radiating out both cranially
358 and caudally. The third dorsobronchus (D3) runs caudodorsally (Fig. 10D) with more large-
359 diameter tertiary bronchi arising from this bronchus in the older ostriches (Fig. 16H). The fourth
360 dorsobronchus (D4) generally mimics D3 anatomically with increased tertiary branching in the
361 larger and older individuals. The more caudal dorsobronchi (D5-11) decrease in overall size,
362 length, and complexity, acquiring more horizontal positions within the gas-exchanging lung
363 (Figs. 10D; 16B, D, F, H).
364   **Laterobronchi** There are a varying number of laterobronchi in the gas-exchanging lung
365 of *S. camelus*; however, there is one large laterobronchus that is markedly larger than the rest
366 (Fig. 10D; 16B, D, F, H). Many of the accessory laterobronchi are so small in diameter that their
367 origins remain unclear. The large laterobronchus emerges from the ventral surface of the
368 primary bronchus, approximately 180˚ opposite either the 3rd or 4th dorsobronchus. The ostium
369 diameter is more than twice that of its opposing dorsobronchus (SI Table 1) and larger even
370 than the ostium of V1. In all individuals examined, the large laterobronchus is subcircular in
371 cross-section and runs caudoventrally, enlarging into the caudal thoracic air sac. The accessory
372 laterobronchi vary in size and shape, all emerge from the ventral and ventrolateral surfaces of
373 the primary bronchus and are angled caudoventrally towards the ventral surface of the gas-
374 exchanging lung.
375   **Primary, secondary, and tertiary expansions (air sacs)** The anatomy of the air sacs in
376 the ostrich have been described elsewhere (Bezuidenhout et al., 1999); however, there are
377 specific aspects of the air sacs worth noting that have not yet been described. Developmental
378 studies of chicks indicate that the air sacs are dilations of the bronchial tree that extend past
379 the margin of the respiratory parenchyma, or "gas-exchanging" lung (Locy and Larsell, 1916a).
380 The abdominal air sac is a caudally projecting expansion of the caudal aspect of the
381 intrapulmonary primary bronchus as it reaches the caudal aspect of the gas-exchanging lung
382 (Fig. 9; 12). Our imaging data demonstrate that the caudal thoracic sacs are the expanded distal
383 aspects of the large laterobronchus. The cranial thoracic and cervical sacs are expansions of the
384 first two ventrobronchi, and in some individuals were merged into one large sac (ostrich 6; Fig.
385 9C). The interclavicular sac, which completely envelops the ventral and lateral surfaces of the
386 syrinx, is an expansion of the medial branches of the cranial ventrobronchi (ostrich 7; Fig. 12E).
387   **Pulmonary diverticula** Müller (Müller, 1908) described and named numerous diverticula
388 that extended from the air sacs and the gas-exchanging lung of the pigeon, which variably
389 pneumatize adjacent skeletal tissues. These have also been observed and described in many
390 other avian taxa including the turkey (*Meleagris gallopavo*), the blackheaded gull (*Larus
391 ridibundus*), anseriform birds, and the Trochilidae (Cover, 1953, King, 1966, King and McLelland,
392 1975, McLelland, 1989, O'Connor, 2004). These diverticula are large and clearly present in the
393 ostrich; however, they diverge from the descriptions published for other taxa in a few ways. In

394 other birds, there are diverticula cranial to the immobilized gas-exchanging lung that are
395 described as emerging from the cervical air sacs and traveling cranially up the cervical
396 vertebrae, often pneumatizing the adjacent skeletal tissues (King, 1966, McLelland, 1989,
397 O'Connor, 2004). King (1966) illustrated these diverticula in *Gallus domesticus* as projecting
398 from the dorsal surface of the cervical sac, with no connection to the gas-exchanging lung. In
399 the ostrich, the vertebral diverticula emerge directly from the cranial margin of the gas-
400 exchanging lung and are situated dorsally to what appear to be the true cervical sacs (Figs. 12A,
401 B; 13; 14). It is highly likely that there are interconnections between the cervical sacs and these
402 diverticula, but a clear origin of the vertebral diverticula directly from the cervical sacs is not
403 supported by these CT-based data. It is important to note that Bezuidenhout et al. (1999) and
404 Fowler (1991) describe the ostrich as being apneumatic aside from the femur alone (citing older
405 literature); however, our data are in agreement with O'Connor and Claessens (2005) and
406 demonstrate that the entire vertebral column, ilia, and femora are pneumatized in the larger
407 ostriches and adult specimen (Fig. 15; see the full set of DICOM data available via Data Dryad to
408 evaluate the extent of the pneumaticity in *S. camelus*). Addressing this requires use of latex
409 injection and a better understanding of embryonic development so that boundaries and origins
410 between specific sacs and diverticula can be confidently identified.
411   With respect to the abdominal region in the pigeon, Müller (1908) found that there are
412 numerous diverticula, termed 'diverticula pelvica' and 'inguinalia', that emerge directly from
413 the abdominal sac itself. The diverticula pelvica is described as surrounding the kidneys, and
414 sending multiple processes cranially and caudally, with a few entering and pneumatizing the
415 ilium and sacrum. The diverticula inguinalia are also described as emerging from the abdominal
416 sac, surrounding the femoral head and sending extensions between the muscles of the thigh
417 (Müller, 1908). According to Müller, Gadow (1891) describes numerous openings of the
418 secondary bronchi emerging from the surface of the lung that form into sacs, but Müller
419 discounts this as an aberrant specimen. The pelvic diverticula described for Anseriformes also
420 appear to follow this pattern (O'Connor, 2004), as do numerous other avian taxa (McLelland,
421 1989). In the ostrich, the pelvic diverticula appear to emerge directly from the caudal aspect of
422 the gas-exchanging lung, and do not demonstrate any clear large connections to the abdominal
423 sacs (ostrich 7; Figs. 13; 14). These pelvic diverticula seemingly directly pneumatize the adjacent
424 pelvic and femoral skeletal elements, not the abdominal air sac as described for most birds
425 (O'Connor, 2004). However, this observation requires validation via latex injection to ensure
426 preservation of the thin septa of avian air sacs.
427
428 **Pulmonary measures**
429   The majority of lung metrics (primary bronchus area, ostium area, distance from the
430 carina to the secondary bronchi) grew isometrically with respect to body size in both *A.*
431 *mississippiensis* and *S. camelus* (Figs. 17 – 21, Tables 5 and 6). However, the area of the primary
432 bronchus (Fig. 17A) at the CVB, the area of the ostium of the CVB (Fig. 17B), and the area of the
433 primary bronchus at D3 (Fig. 19A) were negatively allometric in *A. mississippiensis*. The area of
434 the ostium of V1 (Fig. 17B), area of the primary bronchus and ostium of D1 (Fig. 18A), area of
435 the ostium of D2 (Fig. 19B), and the area of the ostium of L1 (Fig. 21B) were positively
436 allometric in *S. camelus*. The area of the ostium of CVB/V1 (Fig. 17B), the area of the primary
437 bronchus and ostium of D2/D1 (Fig. 18A, B), the area of the primary bronchus of D3/D2 (Fig.
438 19A), and the area of the ostium of L1 (Fig. 21B) were significantly different between *A.*
439 *mississippiensis* and *S. camelus*. Linear metrics (e.g., distance to carina) have isometric slopes of

440   0.33 when compared with body mass, while area metrics (e.g., ostium area) have isometric
441   slopes of 0.66 when compared with body mass (Tables 5 – 7).
442   To generalize lung proportions across a range of body sizes, the distances from the
443   carina to the bronchi were converted into ratios of total length of the primary bronchus (carina
444   to D5 in *A. mississippiensis* and D4 in *S. camelus*) (Fig. 22). The mean distance from the carina to
445   the CVB/V1 is 45.02% (SD = 2.67) total length in *A. mississippiensis* and 48.06% (SD = 2.87) total
446   length in *S. camelus* (Fig. 22). The mean distance of the CVB/V1 to D2/D1 is 12.44% (SD = 1.76)
447   total length in *A. mississippiensis* and 31.12% (SD = 1.69) total length in *S. camelus*. The mean
448   distance of D2/D1 to D3/D2 is 13.91% (SD = 1.89) total length in *A. mississippiensis* and 7.51%
449   (SD = 0.83) total length in *S. camelus.* The mean distance of D3/D2 to D4/D3 is 13.65% (SD =
450   2.26) total length in *A. mississippiensis* and 6.65% (SD = 0.68) total length in *S. camelus*. The
451   mean distance of D4/D3 to D5/D4 is 14.97% (SD = 2.49) total length in *A. mississippiensis* and
452   6.65% (SD = 0.65) total length in *Struthio.*
453
454   **DISCUSSION**
455   **Intra- and interspecific variation**
456   All of the alligators demonstrated some bilateral asymmetry in their bronchial tree,
457   particularly in the overall morphology of the tertiary bronchi, caudal group bronchi (CGB), and
458   caudal medial bronchi (Fig. 8). The number of dorsobronchi remained relatively constant with
459   seven of the ten individuals having four dorsobronchi on both sides (Table 2). All of the
460   alligators had paired M1 branches that were anatomically similar; however, M2 and the more
461   caudal medial bronchi varied from left to right in all of the individuals. In all of the alligators
462   examined, the primary cardiac lobe (i.e., the more cranial lobe that occupied the space
463   between the carina and hila) emerged from the right lung. However, the number of bronchi
464   that contributed to each cardiac lobe was highly variable, ranging from one on the left and two
465   on the right in *A. mississippiensis* 11 to up to four in the left lung in *A. mississippiensis* (Table 2).
466   The overall size of the right and left lungs relative to one another was approximately equal in
467   the majority of individuals examined, with three animals exhibiting a slightly larger left lung.
468   Considering that two of the three alligators with unequal lungs were inflated outside of the
469   body, it is difficult to determine whether or not this difference was artifactual.
470   Like the alligators, all of the ostriches demonstrated some bilateral bronchial
471   asymmetry. The number and size of the accessory laterobronchi (i.e., the small diameter
472   laterobronchi) varied from individual to individual (Fig. 16). The number of dorsobronchi also
473   varied and estimates for the minimal number of branches indicated both intraspecific variation
474   as well as some left to right asymmetry (Table 3). One *S. camelus* even appeared to have an
475   extra dorsobronchus cranial to what was identified as the first dorsobronchus (based upon its
476   position on the primary bronchus and extreme bilateral asymmetry). The number and
477   morphology of the ventrobronchi was more consistent in the ostriches with the majority of
478   individuals displaying four paired ventrobronchi (8/11 individuals); however, two *S. camelus*
479   possessed five ventrobronchi in both lungs, and one *S. camelus* had five ventrobronchi in the
480   right lung and four in the left (Table 3).
481   Variation was evident in the bronchial tree of both *A. mississippiensis* and *S. camelus*
482   with the most variation arising in the caudal and ventral regions of the lung in both taxa. Based
483   on the presence of variation in the structure and number of the secondary airways, it is likely
484   that the total number of dorsobronchi in birds and crocodilians does not have an impact on the
485   direction of airflow. The ventrobronchi appeared to be more tightly constrained in number; one

486 bronchus (functionally, with respect to flow) in the alligators (Farmer and Sanders, 2010) and
487 either four or five in ostriches (Table 3). This difference is not surprising considering that
488 ventrobronchi have been hypothesized to play a significant role in the inspiratory valve of the
489 avian bronchial tree (Butler et al., 1988, Harvey and Ben-Tal, 2016, Maina and Africa, 2000,
490 Maina et al., 2009, Wang et al., 1988). The distance between the carina and each of the major
491 secondary bronchi in both taxa showed minimal intraspecific variation (Fig. 22), suggesting that
492 the spacing between the secondary bronchi may be functionally constrained. These distances
493 may also be ancestrally constrained for Archosauria, and thus could be reconstructed in the
494 ancestral lung, if present in a broad range of extant avian and crocodilian taxa.
495   The most unambiguous differences between the bronchial tree of alligators and
496 ostriches is that in alligators, all of the bronchi are contained within the gas-exchanging lung.
497 However, in ostriches (as in all other birds) "extrapulmonary" extensions of the bronchial tree
498 extend beyond the immobilized gas-exchanging lung, forming the compliant ventilatory air sacs.
499 Distinct similarities are visually evident in the developing chicken lung (*Gallus gallus*) before the
500 air sacs extend beyond the margin of the gas-exchanging lung (Fig. 23). Depending upon the
501 hypotheses of homology used (see below), the general pattern exhibited by our data and that
502 of previous studies (Farmer and Sanders, 2010, Sanders and Farmer, 2012, Schachner et al.,
503 2013), is that *A. mississippiensis* exhibited only one ventrobronchus (CVB), whereas the ostrich
504 had four to five. The alligators also possessed fewer dorsobronchi (three or four) compared to
505 the seven to eleven identified in the ostriches. One of the clear differences between alligator
506 and ostrich lungs in general, aside from the number of large secondary bronchi, is in the path
507 and morphology of the primary bronchus. In all of the ostriches examined, the intrapulmonary
508 primary bronchus begins with a large area, and tapers caudally until it eventually leaves the
509 gas-exchanging lung, ballooning into the abdominal air sac (Figs. 9D; 12E). In alligators, the
510 intrapulmonary primary bronchus is constricted proximally, and expands within the lung (Fig. 7)
511 caudal to the ostium of D3 (the second dorsobronchus), looping medially to form a hook-like
512 structure with secondary sac-like bronchi emerging off of its caudal margin. It has been
513 proposed that the balloon-like expansion emerging from the caudalmost aspect of this hook,
514 which is also present in the Nile crocodile (*Crocodylus niloticus*), is homologous to the
515 abdominal air sac in birds (Schachner et al., 2013). Additionally, ventrobronchi 2–4 (or 5) in the
516 ostrich travel medially and caudally in all of the birds examined. In one of the alligators, there
517 was a small secondary tube-shaped branch emerging from the base of the CVB, and in many
518 alligators the secondary bronchi emerging from the CVB varied dramatically in morphology,
519 ranging from elongated tubes to voluminous sacs (Fig. 8C, F, I, L), suggesting that there may be
520 some plasticity in the development of the number of CVB/ventrobronchi in both taxa.
521   The interspecific comparison is between an ontogenetic series, but no age data were
522 available for these specimens, so it is not possible to make direct comparisons of growth
523 relative to age across the two taxa, only size. Of fifteen lung metrics, five were significantly
524 different between the alligator and ostrich (Table 7). The area of the primary bronchus and
525 ostia increased isometrically or negatively allometrically in alligators and isometrically or
526 positively allometrically in ostriches with respect to body mass (Figs. 17A-B; 18 A-B; 19 A-B; 20
527 A-B; 21; Tables 5, 6). In both taxa, the distances from the carina to the secondary bronchi
528 increased isometrically with mass (Fig. 22), suggesting either phylogenetic or functional
529 constraints. No metrics were positively allometric in *A. mississippiensis* and no metrics were
530 negatively allometric in *S. camelus* suggesting different pulmonary growth trajectories in the
531 bronchial trees in these two taxa.

532   In all of the alligators, the cross sectional area of the intrapulmonary primary bronchus
533   caudal to the hilus increases as the bronchus courses caudally, as reported by others (Sanders
534   and Farmer 2012, Farmer 2015) (Fig. 6), whereas in the ostrich, a different pattern occurs: the
535   area of the primary bronchus appears to decrease caudal to the first few dorsobronchi (Fig. 11);
536   however, metrics were not collected on this region of the primary bronchus. It is unclear what
537   these bronchial metrics mean biologically or physiologically, but these data provide an
538   infrastructure to begin intra- and interspecific quantitative and qualitative comparisons across
539   Archosauria.
540
541   **Pulmonary heterogeneity and hypotheses of homology in the archosaurian lung**
542   The extreme heterogeneity of the avian respiratory system has been well documented
543   since the late 19th century (Duncker, 1971, Huxley, 1882). However, there is confusion within
544   the literature in the nomenclature surrounding the separation between the gas-exchanging
545   portion of the lung and the non-gas exchanging regions of the lung. Historically, the gas-
546   exchanging lung has always been termed the "lung," while the non-gas-exchanging regions are
547   identified as "air sacs." The functional difference between the gas-exchanging portion of the
548   lung and the air sacs necessitates this distinction; however, it is important to note that the
549   entire post-tracheal respiratory apparatus is indeed, the lung. It is clear from work on avian
550   lung development (Locy and Larsell, 1916a, Locy and Larsell, 1916b) that the avian air sacs are
551   secondary and tertiary expansions of the bronchial tree and thus are a part of the lung proper,
552   as in other vertebrates. This has been demonstrated developmentally in the chicken (*Gallus*
553   *gallus domesticus*) when the air sacs first emerge off of the bronchial tree at day four of
554   incubation before they extend beyond the boundary of the gas-exchanging lung (Fig. 23A). In *S.*
555   *camelus*, some of the secondary bronchi emerge beyond the boundaries of the gas-exchanging
556   lung to connect with the air sacs but are not themselves considered part of the air sacs (Fig.
557   10A). This is particularly evident in the ventrolaterally projecting aspect of the first
558   ventrobronchus as it travels down the craniolateral surface of the gas-exchanging lung to
559   expand into the cranial thoracic air sacs (Fig. 10A). This region of V1 is less vascularized than the
560   "lung" proper and would not remain attached to the gas-exchanging lung if it were excised.
561   Thus, it is important to note that the air sacs are just massive expansions of the bronchial tree
562   and should always be considered part of the lung. Despite the structural and functional
563   differentiation of the avian bronchial tree into gas-exchanging and ventilatory regions, distinct
564   similarities to the crocodilian respiratory system become apparent when the lungs are assessed
565   using a comparative approach.
566   Hypotheses of homology between crocodilian and avian lungs were first proposed in
567   1882, when Thomas Henry Huxley made comparisons between the respiratory system of
568   *Apteryx,* an unnamed duck, and crocodiles, even giving a brief mention to the respiratory
569   organs of their dinosaurian ancestors (Huxley, 1882). Global possibilities of homologies
570   between the lung and bronchial tree of the alligator and the avian lung appear particularly clear
571   when alligators are compared with the developing chick respiratory tract at day eight of
572   incubation, prior to when the air sacs emerge beyond the margin of the gas-exchanging portion
573   of the lung (Fig. 23).
574   Sanders and Farmer (Sanders and Farmer, 2012) generated a clear map of potential
575   homologous bronchi shared between *A. mississippiensis* and the chicken (*G. g. domesticus*)
576   based on previous developmental work (Locy and Larsell, 1916a, Broman, 1939), which is what
577   we have followed here (Table 2). In this hypothesis (termed bronchial homology hypothesis 1),

578 the alligator CVB is homologous to all of the avian ventrobronchi collectively, the alligator
579 dorsobronchi (D2–5) are putatively homologous with the avian dorsobronchi (D1–4), and the
580 medial bronchi of the alligator have been lost in the bird or were never shared pulmonary traits
581 (Fig. 24). In the ostrich, all of the ventrobronchi are offset medially from the dorsobronchi in a
582 distinct row, and V2–4 are distinct from V1 in that they do not project far cranially, and
583 predominantly occupy space along caudomedial aspect of the gas-exchanging lung. In all of the
584 alligators, and in *Crocodylus niloticus* (Schachner et al., 2013), there are multiple secondary
585 medial bronchi arising off of the intrapulmonary primary bronchus that are usually left out of
586 homology comparisons or coupled with the dorsobronchi due to similarities in function. After
587 examining the alignment of the dorso- and medial bronchi in the *A. mississippiensis* relative to
588 the ostrich, we propose a possible second alternative hypothesis (bronchial homology
589 hypothesis 2) (Fig. 24). In hypothesis 2, the CVB of alligators remains homologous to V1 of the
590 ostrich, as in hypothesis 1; however, the medial bronchi of alligators are putatively homologous
591 to the avian ventrobronchi 2–4 due to their similar medial alignment along the intrapulmonary
592 primary bronchus (Fig. 24I, K). Functionally, the ventrobronchi of birds operate as the return
593 circuit, taking oxygen-poor air from the parabronchi and delivering it to the trachea for
594 expiration (Brackenbury, 1979, Fedde, 1980, Scheid et al., 1972). Based upon morphological
595 similarities with the adjacent caudal to cranially ventilated dorsobronchi (Farmer and Sanders,
596 2010), airflow in the crocodilian medial bronchi is also likely caudal to cranial, indicating that if
597 "bronchial hypothesis 2" is correct (Fig. 24C, F), there would have been a change in function
598 from delivery-bronchus to return-bronchus in either crocodilians or the avian line. Additional
599 hypotheses associated with the identity and homology of the secondary bronchi and regions of
600 the lung are possible; however, a much broader phylogenetic range of taxa are required to
601 begin to test these hypotheses. Most importantly, developmental experimental research is
602 required to investigate the genetic underpinnings of the branching patterns of the archosaurian
603 bronchial trees.
604
605 **The evolution of the archosaurian respiratory system**
606   Due to the presence of unidirectional airflow in extant crocodilians (Farmer, 2015b,
607 Farmer and Sanders, 2010, Schachner et al., 2013), varanids (Schachner et al., 2014), and
608 iguanas (Cieri et al., 2014), it has become clear that there is no causal relationship between
609 unidirectional airflow patterns and the presence of extra-pulmonary air sacs. This was originally
610 demonstrated by experimental occlusion of the cranial and caudal thoracic sacs, and abdominal
611 sacs of the chicken (Brackenbury and Amaku, 1990, Brackenbury et al., 1989). The presence of
612 aerodynamic valves in birds (Butler et al., 1988), crocodilians (Farmer and Sanders, 2010,
613 Schachner et al., 2013), and varanids (Cieri and Farmer, 2019, Schachner et al., 2014), suggests
614 that this trait is ubiquitous in archosaurs, both extinct and extant, and is likely ancestral for
615 Diapsida (Cieri et al., 2014, Cieri and Farmer, 2016, Farmer, 2015b, Farmer, 2015a, Farmer,
616 2015c, Schachner et al., 2014). The majority of these taxa were not active flyers, demonstrating
617 that unidirectional airflow did not evolve to support the metabolic demands of flight, or of
618 endothermy (Cieri and Farmer, 2016, Farmer, 2015a, Farmer, 2015c). Farmer (2010) proposed
619 the hypothesis that unidirectional flow evolved in basal archosaurs (and perhaps in earlier
620 sauropsids) to facilitate gas exchange during apnea by coupling flow patterns with the beating
621 heart. Farmer (2010) measured unidirectional pulses in airflow that corresponded with
622 individual heartbeats via an ECG in *A. mississippiensis*. Unlike extant mammals, all "reptiles" are
623 known to have long periods of apnea, during which unidirectional airflow would be distinctly

624   advantageous for oxygen extraction, particularly when coupled with cardiogenic airflow
625   patterns (Farmer, 2010).
626   The radiation of Mesozoic archosaurs is one of the most extensively studied (e.g.,
627   Benton and King, 1989, Foth et al., 2016, Benson et al., 2014, Butler et al., 2014), and yet poorly
628   understood diversification events in geologic history. After the Permo-Triassic extinction event,
629   archosaurs were able to diversify and occupy every large-bodied ecological niche,
630   outcompeting mammals until the end of the Mesozoic Era. Reconstruction of the ancestral
631   archosaurian lung necessitates careful analysis of the osteological correlates of relevant extinct
632   taxa. As these correlates only provide information on the external surfaces of the anatomy of
633   the respiratory system that directly contact the adjacent skeletal tissues, the internal
634   pulmonary anatomy can only be inferred from shared characteristics found in the lungs of
635   extant archosaurs. This will provide a starting point for qualitative and quantitative
636   comparisons and evolutionary reconstructions. Certain structural and regional similarities
637   between the bronchial tree of *S. camelus* and *A. mississippiensis* demonstrate that some traits
638   were likely plesiomorphic for Archosauria and may have provided a competitive advantage
639   experienced by archosaurs during the Late Triassic period over the bronchoalveolar lung of
640   mammals, particularly when atmospheric oxygen levels are modeled to have been lower than
641   present conditions and fluctuated during the Mesozoic (see e.g., Berner et al., 2007, Schachat
642   et al., 2019).
643
656
657   **AUTHOR CONTRIBUTIONS**
658
659   ERS and CGF initially designed the project with input from JRH. ERS and CGF collected the scan
660   data. The 2D metrics and 3D models were collected/segmented by ERS. Data analysis was
661   completed by ERS, BPH, HAR, and CGF. Statistical analyses were completed by BPH, with the
662   exception of body mass reconstructions which were done by HAR. All authors contributed to
663   the final synthesis of the data and writing of the manuscript.
664
665   **Literature cited**
666
667   Benson RJB, Campione NE, Carrano MT, et al. (2014) Rates of dinosaur body mass evolution
668   indicate 170 million years of sustained ecological innovation on the avian stem
669   lineage. *PLoS Biology,* **12(5),** e1001853.

670 Benton MJ, King PW (1989) Mass extinctions among tetrapods and the quality of the fossil
671   record (and discussion). *Philosophical Transactions of the Royal Society of London.*
672   *Series B, Biological Sciences,* **325,** 369-386.
673 Berner RA, VandenBrooks JM, Ward PD (2007) Oxygen and Evolution. *Science,* **316,** 557-
674   316.
675 Bezuidenhout AJ, Groenewald HB, Soley JT (1999) An anatomical study of the respiratory
676   air sacs in ostriches. *Onderstepoort Journal of Veterinary Research,* **66,** 317-325.
677 Brackenbury JH (1972) Physical determinants of airflow pattern within the avian lung.
678   *Respiration Physiology,* **15,** 384-397.
679 Brackenbury JH (1979) Corrections to the Hazelhoff model of airflow in the avian lung.
680   *Respiration Physiology,* **36,** 143-154.
681 Brackenbury JH, Amaku J (1990) Effects of combined abdominal and thoracic air-sac
682   occlusion on respiration in domestic fowl. *Journal of Experimental Biology,* **152,** 93-
683   100.
684 Brackenbury JH, Darby C, El-Sayed MS (1989) Respiratory function in exercising fowl
685   following occlusion of the thoracic air sacs. *Journal of Experimental Biology,* **145,**
686   227-237.
687 Broman I (1939) Die Embryonalentwicklung der Lungen bei Krokodilen und
688   Seesschildkröten. *Jb. morphol. mikrosk. Anat.,* **84,** 224-306.
689 Butler JP, Banzett RB, Fredberg JJ (1988) Inspiratory valving in avian bronchi: aerodynamic
690   considerations. *Respiration Physiology,* **72,** 241-256.
691 Butler RJ, Sullivan C, Ezcurra MD, Liu J, Lecuona A, Sookias RB (2014) New clade of
692   enigmatic early archosaurs yields insights into early pseudosuchian phylogeny and
693   the biogeography of the archosaur radiation. *BMC Evolutionary Biology,* **14,** 128.
694 Cieri RL, Crave BA, Schachner ER, Farmer CG (2014) New insight into the evolution of the
695   vertebrate respiratory system and the discovery of unidirectional airflow in iguana
696   lungs. *Proceedings of the National Academy of Science,* **111,** 17218-17223.
697 Cieri RL, Farmer CG (2016) Unidirectional pulmonary airflow in vertebrates: a review of
698   structure, function, and evolution. *Journal of Comparative Physiology B,* **186,** 541-
699   552.
700 Cieri RL, Farmer CG (2019) Computational fluid dynamics reveals a unique net
701   unidirectional pattern of pulmonary airflow in the savannah monitor lizard
702   (Varanus exanthematicus). *The Anatomical Record.*
703 Cover MS (1953) Gross and microscopic anatomy of the respiratory system of the turkey
704   III. The air sacs. *American Journal of Veterinary Research,* **14,** 239-246.
705 Duncker HR (1971) The lung air sac system of birds. A contribution to the functional
706   anatomy of the respiratory apparatus. *Ergebnisse der Anatomie und*
707   *Entwicklungsgeschichte,* **45,** 1-171.
708 Duncker HR (1972) Structure of avian lungs. *Respiration Physiology,* **14,** 44-63.
709 Farmer CG (2006) On the origin of avian air sacs. *Respiration Physiology and Neurobiology,*
710   **154,** 89-106.
711 Farmer CG (2010) The provenance of alveolar and parabronchial lungs: insights from
712   paleoecology and the discovery of cardiogenic, unidirectional airflow in the
713   American alligator (*Alligator mississippiensis*). *Physiological and Biochemical*
714   *Zoology,* **83,** 561-575.
715 Farmer CG (2015a) The evolution of unidirectional pulmonary airflow. *Physiology,* **30,** 260-
716   272.

717   Farmer CG (2015b) Similarity of crocodilian and avian lungs indicates unidirectional flow
718   is ancestral for archosaurs. In *Integrative and Comparative Biology*), pp. 1-10.
719   Farmer CG (2015c) Unidirectional flow in lizard lungs: a paradigm shift in our
720   understanding of lung evolution in Diapsida. *Zoology,* **118,** 299-301.
721   Farmer CG, Sanders K (2010) Unidirectional airflow in the lungs of alligators. *Science,* **327,**
722   338-340.
723   Fedde MR (1980) Structure and gas-flow pattern in the avian respiratory system. *Poultry*
724   *Science,* **59,** 2642-2653.
725   Foth C, Ezcurra MD, Sookias RB, Brusatte SL, Butler JP (2016) Unappreciated diversification
726   of stem archosaurs during the Middle Triassic predated the dominance of dinosaurs.
727   *BMC Evolutionary Biology,* **16,** 188.
728   Fowler ME (1991) Comparative clinical anatomy of ratites. *Journal of Zoo and Wildlife*
729   *Medicine,* **22,** 204-227.
730   Gadow H (1891) Vögel. *In: Bronn's Klass. Ord. Tierreich,* **6**.
731   Gignac PM, Kley NJ, Clarke JA, et al. (2016) Diffusible iodine-based contrast-enhanced
732   computed tomography (diceCT): An emerging tool for rapid, high-resolution, 3-D
733   imaging of metazoan soft tissues. *Journal of Anatomy,* **228,** 889-909.
734   Harvey EP, Ben-Tal A (2016) Robust Unidirectional Airflow through Avian Lungs: New
735   Insights from a Piecewise Linear Mathematical Model. *PloS Computational Biology,*
736   **12,** e1004637.
737   Hedrick BP, Yohe L, Vander Linden A, et al. (2018) Assessing soft-tissue shrinkage
738   estimates in museum specimens imaged with diffusible iodine-based contrast-
739   enhanced computed tomography (diceCT). *Microscopy and Microanalysis,* **24,** 284-
740   291.
741   Huxley TH (1882) On the respiratory organs of *Apteryx*. *Proceedings of the Zoological*
742   *Society of London,* **1882,** 560-569.
743   Jeffery NS, Stephenson RS, Gallagher JA, Jarvis JC, Cox PG (2011) Micro-computed
744   tomography with iodine staining resolves the arrangement of muscle fibres. *Journal*
745   *of Biomechanics,* **44,** 189-192.
746   King AS (1966) Structural and functional aspects of the avian lungs and air sacs. In
747   *International Review of General and Experimental Zoology* (eds Felts JL, Harrison RJ),
748   pp. 96. New York and London: Academic Press.
749   King AS, McLelland J (1975) *Birds-Their Structure and Function,* Bailliere Tindall, London.
750   Locy WA, Larsell O (1916a) The embryology of the bird's lung based on observations of the
751   domestic fowl Part I. *The American Journal of Anatomy,* **19,** 447-506.
752   Locy WA, Larsell O (1916b) The embryology of the bird's lung based on observations of the
753   domestic fowl Part II. *The American Journal of Anatomy,* **20,** 1-44.
754   Maina J (2007) Spectacularly robust! Tensegrity principle explains the mechanical strength
755   of the avian lung. *Respiratory Physiology and Neurobiology,* **155,** 1-10.
756   Maina J, Nathaniel C (2001) A qualitative and quantitative study of the lung of an ostrich.
757   *Journal of Experimental Biology,* **204,** 2313-2330.
758   Maina JN (1989) The morphometry of the avian lung. In *Form and Function in Birds* (eds
759   King AS, McLelland J), pp. 307-368. London: Academic Press.
760   Maina JN (2006a) Development, structure, and function of a novel respiratory organ, the
761   lung-air sac system of birds: to go where no other vertebrate has gone. *Biological*
762   *Reviews,* **81,** 545-579.
763   Maina JN (2006b) Spectacularly robust! Tensegrity principle explains the mechanical
764   strength of the avian lung. *Respiration Physiology & Neurobiology,* **155,** 1-10.

765   Maina JN (2017) Pivotal debates and controversies on the structure and function of the
766   avian respiratory system: setting the record straight. *Biological Reviews,* **92,** 1475–
767   1504.
768   Maina JN, Africa M (2000) Inspiratory aerodynamic valving in the avian lung: functional
769   morphology of the extrapulmonary primary bronchus. *Journal of Experimental*
770   *Biology,* **203,** 2865-2876.
771   Maina JN, Singh P, Moss EA (2009) Inspiratory aerodynamic valving occurs in the ostrich,
772   *Struthio camelus* lung: A computational fluid dynamics study under resting unsteady
773   state inhalation. *Respiration Physiology & Neurobiology,* **169,** 262-270.
774   McLelland J (1989) Anatomy of the lungs and air sacs. In *Form and Function in Birds* (eds
775   King AS, McLelland J), pp. 221-279. London: Academic Press.
776   Müller B (1908) The air-sacs of the pigeon. *Smithsonian Miscellaneous Collections,* **50,** 365-
777   414.
778   O'Connor PMO (2004) Pulmonary pneumaticity in the postcranial skeleton of extant Aves:
779   A case study examining Anseriformes. *Journal of Morphology,* **261,** 141-161.
780   O'Connor PMO, Claessens LPAM (2005) Basic avian pulmonary design and flow-through
781   ventilation in non-avian theropod dinosaurs. *Nature,* **436,** 253-256.
782   Saalfeld DT, Webb KK, Conway WC, Calkins GE, Duguay JP (2008) Growth and condition of
783   American alligators (*Alligator mississippiensis*) in an inland wetland of East Texas.
784   *Southeastern Naturalist,* **7,** 541-550.
785   Sakiyama J, Yokouchi Y, Kuroiwa A (2000) Coordinated expression of *Hoxb* genes and
786   signaling molecules during development of the chick respiratory tract. *Development*
787   *Biology,* **227,** 12-27.
788   Sanders RK, Farmer CG (2012) The pulmonary anatomy of *Alligator mississippiensis* and its
789   similarity to the avian respiratory system. *The Anatomical Record,* **295,** 699-714.
790   Sappey P-C (1847) *Recherches sur L'appareil Respiratoire des Oiseaux,* Germer-Bailliere,
791   Pairs.
792   Schachat SR, Labandeira CC, Saltzman MR, Cramer BD, Payne JL, Boyce CK (2019)
793   Phanerozoic *p*O2 and the early evolution of terrestrial animals. *Proceedings of the*
794   *Royal Society B,* **285,** 20172631.
795   Schachner ER, Cieri RL, Butler JP, Farmer CG (2014) Unidirectional pulmonary airflow
796   patterns in the savannah monitor lizard. *Nature,* **506,** 367-370.
797   Schachner ER, Hutchinson JR, Farmer CG (2013) Pulmonary anatomy in the Nile crocodile
798   and the evolution of unidirectional airflow in Archosauria. *PeerJ*, DOI
799   10.7717/peerj.60.
800   Schachner ER, Sedlmayr JC, Schott R, Lyson TR, Sanders RK, Lambertz M (2017) Data from:
801   Pulmonary anatomy and a case of unilateral aplasia in a common snapping turtle
802   (*Chelydra serpentina*): developmental perspectives on cryptodiran lungs. In *Journal*
803   *of Anatomy*). Dryad Digital Repository.
804   Scheid P, Slama H, Piiper J (1972) Mechanisms of unidirectional flow in parabronchi of
805   avian lungs: measurements in duck lung preparations. *Respiration Physiology,* **14,**
806   83-95.
807   van Buuren S, Groothuis-Oudshoorn K (2011) mice: Multivariate Imputation by Chained
808   Equations in R. *Journal of Statistical Software,* **45,** 1-67.
809   Wang N, Banzett RB, Butler JP, Fredberg JJ (1988) Bird lung models show that convective
810   inertia effects inspiratory aerodynamic valving. *Respiration Physiology,* **73,** 111-124.

811   Witmer LM (1995) The extant phylogenetic bracket and the importance of reconstructing
812   soft tissues in fossils. In *Functional Morphology in Vertebrate Paleontology* (ed
813   Thompson JJ), pp. 19-33. Cambridge: Cambridge University Press.
814
815

816 **Table 1.** Data and CT information for the *Struthio camelus* and *Alligator mississippiensis* specimens included in the analysis. *S.* camelus
817 specimens are accessioned at the Museum of Vertebrate Zoology at Berkeley (MVZ).

Taxon	Specimen number	Origin	CT Date	Mass (kg)	Total length	State of specimen at scan	Notes	Scan parameters	Scan location
Struthio camelus	CS2; MVZ190727	LWH	10/26/2012	0.823	N/A	Deceased inflated	No head	kV 100, mA 400	University of Utah South Jordan Medical Center (UUSJMC)
S. camelus	CS1; MVZ190730	LWH	10/26/2012	0.861	N/A	Deceased inflated		kV 100, MA 400	UUSJMC
S. camelus	CS3; MVZ190733	LWH	10/26/2012	1.125	N/A	Deceased	Did not stay inflated	kV 100, mA 400	UUSJMC
S. camelus	CS4; MVZ190731	LWH	10/26/2012	1.341	N/A	Deceased inflated	Propped up in scanner	kV 100, mA 400	UUSJMC
S. camelus	CS5	LWH	10/26/2012	1.801	N/A	Deceased	Did not stay inflated	kV 100, mA 400	UUSJMC
S. camelus	CS6; MVZ190734	LWH	10/26/2012	2.580	N/A	Deceased inflated	Stained with I_2KI	kV 100, mA 400	UUSJMC
S. camelus	CS7; MVZ190729	LWH	10/26/2012	3.538	N/A	Deceased inflated	Intubation tube tied into trachea	kV 100, mA 400	UUSJMC
S. camelus	CS8	LWH	10/26/2012	5.715	N/A	Deceased		kV 100, mA 400	UUSJMC
S. camelus	CS9; MVZ190288	LWH	10/26/2012	4.471	N/A	Deceased		kV 100, mA 400	UUSJMC
S. camelus	CS10; MVZ190332	LWH	10/26/2012	6.599	N/A	Deceased		kV 100, mA 400	UUSJMC

S. camelus	CS11	Royal Veterinary College, London		71.3	N/A	Deceased	Open to atmosphere	kV 120, mA 100	Royal Veterinary College, London
Alligator mississippiensis	AM041315-1	Rockefeller Wildlife Refuge (RWR)	7/01/2015	0.0757	N/A	Deceased	Lungs inflated in the torso	Scanco µCT 40; kV 55 uA 145	LSU School of Veterinary Medicine
A. mississippiensis	15	RWR	3/16/2012	1.7	N/A	Live, unsedated	Scanned in the prone position	kV 120, mA200	University of Utah Research Park (UURP)
A. mississippiensis	9	RWR	3/16/2012	1.75	N/A	Live, unsedated	Scanned in the prone position	kV 120, mA200	UURP
A. mississippiensis	739	RWR	3/16/2012	2.8	N/A	Live, unsedated	Scanned in the prone position	kV 120, mA200	UURP
A. mississippiensis	12	RWR	12/22/2011	5.44	N/A	Deceased	Lungs excised, inflated; stained with I_2KI	kV 120, mA200	University of Utah Hospital (UUH)
A. mississippiensis	54	RWR	2/06/2012	10 (imputed)	54"	Deceased	Lungs excised, inflated; stained with I_2KI	kV 120, mA200	UUH
A. mississippiensis	11	RWR		11	N/A	Live, unsedated	Scanned in the prone position	kV 120, mA 200	UUH
A. mississippiensis	"Stumpy"	RWR	5/05/2013	13.4 (imputed)	N/A	Live, unsedated	Scanned in the supine position	kV 100, mA 400	UUSJMC
A. mississippiensis	64	RWR	8/20/2012	14.5 (imputed)	64"	Deceased	Lungs inflated in the torso; stained with I_2KI	kV 120, mA200	UURP
A. mississippiensis	81	RWR	12/22/2011	31.5 (imputed)	81"	Deceased	Lungs excised, inflated; stained with I_2KI	kV 120, mA200	UUH

818

819

820 **Table 2.** Proposed homologies in the bronchial trees of *Alligator mississippiensis* and *Struthio*
821 *camelus* utilized for qualitative and quantitative comparisons following previous hypotheses of
822 homology (Sanders and Farmer, 2012, Schachner et al., 2013).

823

Alligator mississippiensis	*Struthio camelus*
Cervical ventral bronchus (CVB)	Ventrobronchus 1 (2-4)
Dorsobronchus 2	Dorsobronchus 1
Dorsobronchus 3	Dorsobronchus 2
Dorsobronchus 4	Dorsobronchus 3
Dorsobronchus 5	Dorsobronchus 4
None	Dorsobronchus 5-11

825

826 **Table 3.** Left to right symmetry in the bronchial tree of *Alligator mississippiensis.* Asterisk
827 indicates the lung from which the dominant, and cranially position cardiac lobe arises. The
828 animals are ranked by body mass (smallest at the top).

829

Alligator ID #	State	Dorsobronchi (Left/Right)	Medial bronchi (Left/Right)	Cardiac lobes (Left/Right)
AM041315-1	Deceased, *in situ*	3/4	4/5	3/3*
15	Live	4/4	4/4	3/3*
9	Live	4/5	2/3	3/2*
739	Live	4/4	4/4	3/3*
12	Excised	5/4	4/3	3/3*
54	Excised	4/4	4/3	3/2*
11	Live	4/4	3/3	1/2*
Stumpy	Live	4/4	4/5	2/2*
64	Deceased, *in situ*	4/4	5/3	4/2*
81	Excised	4/4	3/2	3/3*

830

831 **Table 4.** Left to right symmetry in the bronchial tree of *Struthio camelus*. The number of
832 dorsobronchi is a minimum estimate due to the small size of the caudalmost dorsobronchi and
833 the resolution of the CT scanner. Specimens are ranked by body mass (with the smallest at the
834 top).

835

Struthio camelus ID #	State	Dorsobronchi grossly visible (Left/Right)	Ventrobronchi (Left/Right)
2	Deceased, *in situ*	≥ 9/8	4/4
1	Deceased, *in situ*	≥ 7/7	4/4
3	Deceased, *in situ*	≥ 8/8	4/4
4	Deceased, *in situ*	≥ 9/9	4/4
5	Deceased, *in situ*	≥ 9/8	4/5
6	Deceased, *in situ*	≥ 9/9	4/4
7	Deceased, *in situ*	≥ 9/11	5/5
8	Deceased, *in situ*	≥ 9/9	5/5
9	Deceased, *in situ*	≥ 8/9	4/4
10	Deceased, *in situ*	≥ 7/9	4/4
11	Deceased, *in situ*	≥ 7/8	4/4

836

837 **Table 5.** The SMA regression results for the CVB, D2–D5, and L1–2 with respect to body mass of
838 *Alligator mississippiensis*. Slope, confidence intervals around the slope, and the expectation for
839 isometry are reported for each metric. Primary bronchus (PB) area and ostium area are
840 isometric at a slope of 0.66 while distances are isometric at a slope of 0.33.

841

Alligator mississippiensis	Lower CI	Slope	Upper CI	Isometry	Allometry
CVB PB Area	0.485	0.576	0.685	0.66	Iso
CVB Ostium Area	0.457	0.534	0.624	0.66	**Neg**
CVB Distances	0.232	0.289	0.361	0.33	Iso
D2 PB Area	0.456	0.511	0.572	0.66	**Neg**
D2 Ostium Area	0.501	0.563	0.634	0.66	**Neg**
D2 Distances	0.241	0.292	0.354	0.33	Iso
D3 PB Area	0.438	0.501	0.573	0.66	**Neg**
D3 Ostium Area	0.422	0.580	0.796	0.66	Iso
D3 Distances	0.247	0.302	0.370	0.33	Iso
D4 PB Area	0.395	0.562	0.799	0.66	Iso
D4 Ostium Area	0.408	0.558	0.762	0.66	Iso
D4 Distances	0.247	0.304	0.374	0.33	Iso
D5 Distances	0.236	0.294	0.366	0.33	Iso
L1 Ostium Area	0.237	0.364	0.559	0.66	Iso
L2 Ostium Area	0.297	0.498	0.835	0.66	Iso

842

843 **Table 6.** The SMA regression results for the CVB, D2–D5, and L1–2 with respect to body mass of
844 *Struthio camelus*. Slope, confidence intervals around the slope, and the expectation for
845 isometry are reported for each metric. Primary bronchus (PB) area and ostium area are
846 isometric at a slope of 0.66 while distances are isometric at a slope of 0.33.

847

Struthio camelus	Lower CI	Slope	Upper CI	Isometry	Allometry
V1 PB Area	0.610	0.837	1.149	0.66	Iso
V1 Ostium Area	0.704	0.881	1.104	0.66	**Pos**
V1 Distances	0.308	0.361	0.422	0.33	Iso
D1 PB Area	0.660	0.878	1.166	0.66	**Pos**
D1 Ostium Area	0.752	1.009	1.352	0.66	**Pos**
D1 Distances	0.327	0.372	0.424	0.33	Iso
D2 PB Area	0.641	0.913	1.300	0.66	Iso
D2 Ostium Area	0.688	0.925	1.243	0.66	**Pos**
D2 Distances	0.330	0.377	0.430	0.33	Iso
D3 PB Area	0.652	0.958	1.407	0.66	Iso
D3 Ostium Area	0.600	1.019	1.732	0.66	Iso
D3 Distances	0.330	0.376	0.428	0.33	Iso
D4 Distances	0.329	0.376	0.431	0.33	Iso
L1 Ostium Area	1.198	1.514	1.914	0.66	**Pos**
L2 Ostium Area	0.613	0.898	1.317	0.66	Iso

848
849

850   **Table 7.** Comparisons between slopes for *A. mississippiensis* and *S. camelus*. Significant
851   differences determined based on non-overlapping 95% confidence intervals of SMA
852   regressions.
853

	Sig. diff.
CVB/V1 PBArea	
CVB/V1 OstArea	√
CVB/V1 Dist	
D2/D1 PBArea	√
D2/D1 OstArea	√
D2/D1 Dist	
D3/D2 PBArea	√
D3/D2 OstArea	
D3/D2 Dist	
D4/D3 PBArea	
D4/D3 OstArea	
D4/D3 Dist	
D5/D4 Dist	
L1 OstArea	√
L2 OstArea	

854
855   **Supplemental Information Table Captions**
856
857   **SI Table 1** Raw metrics obtained from the lungs of *Struthio camelus* specimens. Colors
858   correspond to hypothesis of homology with the American alligator (*A. mississippiensis*).
859
860   **SI Table 2** Raw metrics obtained from the lungs of the *A. mississippiensis* specimens. Colors
861   correspond to hypothesis of homology with *S. camelus*.
862
863   **SI Table 3** Imputed mass values for each of the four *A. mississippiensis* that had an unknown
864   mass.

865   **Figure captions**

866

867   **Figure 1. Phylogeny for Tetrapoda demonstrating the structural diversity of the tetrapod lung.**
868   A) Amniota; B) Sauropsida; C) Archosauria. Volume rendered skeleton and surface model of the
869   bronchial tree of: D) *Xenopus sp.*; E) *Saguinus sp.*, (with a diagrammatic illustration of a
870   standardized primate bronchial tree); F) *Iguana iguana* (modified from (Cieri et al., 2014); G)
871   *Varanus exanthematicus* (modified from (Schachner et al., 2014); H) *Chelydra serpentina*
872   (modified from Schachner et al., (Schachner et al., 2017); I) *Alligator mississipiensis*; and, J)
873   *Struthio camelus.* Images not to scale.

874

875   **Figure 2. Segmented 3D surface model of the thorax, lung, and bronchial tree of *A.***
876   ***mississippiensis.*** *A. mississippiensis* 11 (live) during a natural apnea in dorsal (A, C, E), and left
877   lateral (B, D, F) views. Parabronchi (i.e., connections between the primary, secondary and
878   tertiary bronchi) are not shown.

879

880   **Figure 3. Diagrammatic models demonstrating the quantitative metrics.** Simplified and
881   reduced digital model of the bronchial tree of the right lung of *Alligator mississippiensis* in
882   medial (A), craniomedial (B), and ventral (C, D) views, with the tertiary, medial, caudal and
883   lateral bronchi all removed. Simplified and reduced digital model of the bronchial tree of the
884   right lung of *Struthio camelus* in (E, F), dorsomedial (G), and ventral (H, I) views. These models
885   are 3D representations and indications of the 2D quantitative metrics obtained from the DICOM
886   images in OsiriX. A) Gold rings represent the metrics obtained at the trachea (metric 1) and
887   primary bronchus (metric 2) in the alligator. Pink oblique rings demonstrate the sites where
888   metrics were taken for the area of the primary bronchus, perpendicular to the origin of the
889   secondary bronchus (metric 3). B) Red oblique rings represent the site where the metrics were
890   taken for the area of the ostium for each secondary bronchus as it branched from the primary
891   bronchus (metric 4). C-D) Diagram of where metrics were taken for the distances from the
892   carina to each of the large secondary bronchial ostia (metric 6) (C) with the bronchi labeled (D)
893   (metrics 1 and 2 are also labeled in this view). E) Pink oblique circles demonstrating the position
894   of metric 3 in the ostrich. Blue oblique circle demonstrates metric 5 as measured around the
895   large laterobronchus on *S. camelus*. F-G) Red rings demonstrate metric 4 in *S. camelus* for the
896   ventrobronchi and dorsobronchi. H-I) Diagram of where metrics were taken for the distances
897   from the carina to each of the large secondary bronchial ostia (metric 6) in *S. camelus* with the
898   measurement diagram (H) and the labeled ostia (I). Abbreviations: CA, carina; CVB, cervical
899   ventral bronchus; D2-D5, dorsobronchi 2-5; L, laterobronchus; PB, primary bronchus; V1-4,
900   ventrobronchi 1-4. Numbers indicate specific metrics described in methods. Images not to
901   scale.

902

903   **Figure 4. Measured and imputed body masses of *A. mississippiensis* scaled to pulmonary**
904   **measures across a growth series.** (A) Measured/imputed body mass scaled to the maximum
905   diameter of the right primary bronchus just distal to the bifurcation from the trachea; (B)
906   measured/imputed body mass scaled to the area of the right primary bronchus at the same
907   location as (A).

908

909   **Figure 5. Segmented 3D surface model of the primary, secondary, and large tertiary airways**
910   **of *A. mississippiensis* 64.** Specimen is deceased, artificially inflated, and all images in left

911　craniolateral view (except for D). A) The primary, secondary, and large tertiary bronchi; B) the
912　primary and secondary bronchi (the tertiary bronchi have been removed); C) the primary
913　bronchi, the cervical ventral bronchus, and the dorsobronchi; D) image (C) in left lateral view; E)
914　the primary and medial (M) bronchi; F) the primary bronchi, the laterobronchi, the cardiac
915　lobes, and the caudal group bronchi. Parabronchi (i.e., connections between the primary,
916　secondary and tertiary bronchi) are not shown. Abbreviations = C, cardiac lobes; CGB, caudal
917　group bronchi; CVB, cervical ventral bronchus; D2-5, dorsobronchi 2-5; L, laterobronchi; M1-5,
918　medial bronchi; Pb, primary bronchus.
919
920　**Figure 6. Segmented 3D surface model of the bronchial tree of *A. mississippiensis* 64.**
921　Bronchial tree in dorsal (A) and ventral (B) views, with the ostia of the major secondary and a
922　few tertiary branches represented as stumps to visually demonstrate clear branching pattern.
923　Abbreviations: C1-4, cardiac lobes 1-4; CVB, cervical ventral bronchus; CVB2, secondary
924　branches off of the cervical ventral bronchus; D2-5, dorsobronchi 2-5; LB, laterobronchi; M1-5,
925　medial bronchi 1-5.
926
927　**Figure 7. Segmented 3D surface model of the dorsal vertebrae and ribs, lung surface, and**
928　**bronchial tree of a hatchling *A. mississippiensis* (AM041315-1) and CT images of a live adult**
929　**("Stumpy").** Hatchling thorax model in left craniolateral (A-C) and ventral (D-F) views generated
930　from µCT data. Lung surface and axial skeleton are shown in (A), (D), and (E). Surface of the
931　lungs and the tertiary bronchi of the left lung are made semi-translucent in (B-C) and (E-F) to
932　demonstrate the position of the major primary and secondary airways within the lung and
933　relative to the smaller interconnecting branches (=parabronchi). Lung surface and tertiary
934　bronchi are removed from the left lung, and the tertiary are made semi-translucent in (C) and
935　(F) to further demonstrate these relationships. Axial (G) and parasagittal (H) CT images of a live
936　adult *A. mississippiensis* (scanned in a supine position) demonstrating the pulmonary
937　heterogeneity and regional distribution of the parenchyma within the lung. Abbreviations: CVB,
938　cervical ventral bronchus; P, parenchyma.
939
940　**Figure 8. Intraspecific and methodological variation in the bronchial tree of *Alligator***
941　***mississippiensis*.** Segmented 3D surface models of the bronchial tree of four different
942　individuals. Top row: The lungs of alligator 81 (deceased), shown in dorsal (A), ventral (B), and
943　left lateral (C) views, were completely dissected out of the thorax, and inflated via a syringe
944　prior to scanning. Second row: alligator 64 (deceased), shown in dorsal (D), ventral (E), and left
945　lateral (F) views, was inflated via a syringe, and scanned *in situ* in the torso. Third row:
946　"Stumpy," shown in dorsal (G), ventral (H), and left lateral (I) views, was scanned live,
947　unsedated, and in an upside down (supine) position. Bottom row: alligator 15, shown in dorsal
948　(J), ventral (K), and left lateral (L) views, was scanned live, unsedated, and prone position.
949　Images not to scale.
950
951　**Figure 9. Segmented 3D surface model of the postcranial skeleton and respiratory system of**
952　***Struthio camelus* 6 (deceased, artificially inflated).** *S. camelus* model in left lateral (A), dorsal
953　(B), and left craniolateral (C-D) views. No secondary pulmonary diverticula are shown. C) Lung
954　surface and air sacs. D) Lung surface has been removed showing a solid representation of the
955　bronchial tree and the direct connections to the extrapulmonary air sacs. Note that the
956　parabronchi are not shown (connections between the dorsobronchi and ventrobronchi) as they

957 are too small to be segmented from the CT data due to resolution of a medical grade scanner.
958 Additionally, the interclavicular and cervical air sacs have been segmented as a single unit due
959 to the inability to differentiate between the boundaries due to the resolution of the scan.
960 Abbreviations: AAS, abdominal air sac; CRTS, cranial thoracic air sac; CS, cervical air sac; CTS,
961 cranial thoracic air sac; GL, gas exchanging lung; IAS, interclavicular air sac.

962

963 **Figure 10. Segmented 3D surface model of the gas exchanging lung and bronchial tree of *S.**
964 ***camelus* 6.** Model is shown in left craniolateral (A-C) and left lateral (D) views. The surface of
965 the gas exchanging lung is represented as semi-translucent blue and the negative space within
966 the bronchial tree is shown as solid. Note that the parabronchi are not shown (connections
967 between the dorsobronchi and ventrobronchi) as they are too small to be segmented from the
968 CT data due to resolution of a medical grade scanner. Abbreviations: CRTS, cranial thoracic air
969 sac; D1-8, dorsobronchi 1-8; LB, laterobronchi; LS, lung surface; PB, primary bronchus; TR,
970 trachea; V1-4, ventrobronchi 1-4.

971

972 **Figure 11. Segmented 3D surface model of the bronchial tree of *S. camelus* 6.** Model is shown
973 in dorsal (A), ventral (B), and left dorsolateral (C) views, with the ostia of the major secondary
974 branches represented as stumps to visually demonstrate clear branching patterns.
975 Abbreviations: CR, carina; D1-7, dorsobronchi 1-7; LB, laterobronchi; PB, primary bronchus; T,
976 trachea; V1-4, ventrobronchi 1-4.

977

978 **Figure 12. Segmented 3D surface model of the entire respiratory system of *S. camelus* 7.**
979 Model is shown in left craniolateral (A, C, D) and lateral views (B, E). The pulmonary diverticula
980 are visible in (A) and (B) and can be clearly seen extending cranially and caudally to the gas-
981 exchanging lung, as well as positioned dorsally to the ventilatory air sacs. The pulmonary
982 diverticula are removed in (C-E) and demonstrate the lack of continuity with the air sacs.
983 Abbreviations: AAS, abdominal air sac; CS, cervical air sac; CRTS, cranial thoracic air sac; CTS,
984 caudal thoracic air sac; D1-2, dorsobronchi 1-2; IAS, interclavicular air sac; L, laterobronchus;
985 PB, primary bronchus; TR, trachea; V1, ventrobronchus 1. Images not to scale.

986

987 **Figure 13. Segmented 3D surface model of the skeleton and respiratory system of *S. camelus***
988 **7.** Model is shown in left craniolateral (A), left lateral (B), right lateral (C), and left dorsolateral
989 views with the left ilium removed (D). The pulmonary diverticula are visualized as a solid in (D)
990 to clarify the relationships between these structures and the adjacent skeletal tissues.

991

992 **Figure 14. Segmented 3D surface model of the gas-exchanging lung, bronchial tree, and**
993 **pulmonary diverticula of *S. camelus* 7.** Model is shown in left lateral view, demonstrating the
994 origin of the majority of the diverticula from the secondary airways, and directly from the
995 surface of the lung, but distinct from the caudal extent of the primary bronchus as it extends
996 beyond the gas-exchanging lung to balloon into the abdominal air sac. Abbreviations: GL, gas
997 exchanging lung; L, laterobronchus; PB, primary bronchus; TR, trachea; V1-2, ventrobronchi 1-2.

998

999 **Figure 15. Volume rendered model and coronal CT slices of *S. camelus* 10 demonstrating**
1000 **extensive axial and appendicular postcranial pneumaticity.** (A) Volume rendered 3D model of
1001 a juvenile *S. camelus* in left lateral view with lines demonstrating the location of the two
1002 coronal DICOM slices shown at positions (B) and (C), and two axial slices shown at positions (D)

1003   and (E). Abbreviations: D, diverticula; DP, diverticula pelvica; F(p), femur (pneumatized); GL,
1004   gas-exchanging lung; R(p), rib (pneumatized); V(p), vertebra (pneumatized).
1005
1006   **Figure 16. Intraspecific variation in the bronchial tree of *Struthio camelus*.** Segmented 3D
1007   surface models of *S. camelus 7* in dorsal (A) and left lateral (B) views, *S. camelus* 8 in dorsal (C)
1008   and left lateral (D) views, *S. camelus* 10 in dorsal (E) and left lateral (F) views, and *S. camelus* 11
1009   in dorsal (G) and left lateral (H) views. Images not to scale.
1010
1011   **Figure 17. Standard major axis regressions of the log of body mass and the log of the**
1012   **following anatomical measurements:** (A) Cross sectional area of intrapulmonary primary
1013   bronchus at the level of CVB (alligator) and V1 (ostrich), (B) cross sectional area of ostium of
1014   CVB and V1 (C) distance from the carina to the ostium of the CVB and V1. (D) Diagrammatic
1015   illustration of the *A. mississippiensis* bronchial tree with the cervical ventral bronchus
1016   highlighted in green. (E) Diagrammatic illustration of the bronchial tree of *S. camelus* with the
1017   cervical ventral bronchus highlighted in green. Abbreviations: CVB, cervical ventral bronchus;
1018   PB, primary bronchus; V1, ventrobronchus. Ostriches = magenta circles. Alligators = blue
1019   triangles.
1020
1021   **Figure 18. Standard major axis regressions of the log of body mass and the log of the**
1022   **following anatomical measurements:** (A) Cross sectional area of intrapulmonary primary
1023   bronchus at the level of D2 (*Alligator*) and D1 (*Struthio*) and body mass (B) cross sectional area
1024   of ostium of the D2 and D1 (C) distance from the carina to the ostium of D2 and D1 (D)
1025   Diagrammatic illustration of the *A. mississippiensis* bronchial tree with dorsobronchus 2 (the
1026   first dorsobronchus) highlighted in lime. (E) Diagrammatic illustration of the bronchial tree of *S.
1027   camelus* with dorsobronchus 1 highlighted in lime. Ostriches = magenta circles. Alligators = blue
1028   triangles.
1029
1030   **Figure 19. Standard major axis regressions of the log of body mass and the log of the**
1031   **following anatomical measurements:** (A) Cross sectional area of intrapulmonary primary
1032   bronchus at the level of D3 (*Alligator*) and D2 (*Struthio*) and body mass (B) cross sectional area
1033   of ostium of the D3 and D2 (C) distance from the carina to the ostium of D3 and D2 (D)
1034   Diagrammatic illustration of the *A. mississippiensis* bronchial tree with dorsobronchus 3 (the
1035   second dorsobronchus) highlighted in neon green. (E) Diagrammatic illustration of the bronchial
1036   tree of *S. camelus* with dorsobronchus 2 highlighted in neon green. Ostriches = magenta circles.
1037   Alligators = blue triangles.
1038
1039   **Figure 20. Standard major axis regressions of the log of body mass and the log of the**
1040   **following anatomical measurements:** (A) Cross sectional area of intrapulmonary primary
1041   bronchus at the level of D4 (*Alligator*) and D3 (*Struthio*) and body mass (B) cross sectional area
1042   of ostium of the D4 and D3 (C) distance from the carina to the ostium of D4 and D3 (D)
1043   Diagrammatic illustration of the *A. mississippiensis* bronchial tree with dorsobronchus 4 (the
1044   third dorsobronchus) highlighted in aqua. (E) Diagrammatic illustration of the bronchial tree of
1045   *S. camelus* with dorsobronchus 3 highlighted in aqua. Ostriches = magenta circles. Alligators =
1046   blue triangles.
1047

1048 **Figure 21. Standard major axis regressions of the log of body mass and the log of the**
1049 **following anatomical measurements:** (A) Cross sectional area of intrapulmonary primary
1050 bronchus at the level of D5 (*Alligator*) and D4 (*Struthio*) and body mass (B) cross sectional area
1051 of the ostium of laterobronchus 1 (C) cross sectional area of the ostium of laterobronchus 2 (D)
1052 Diagrammatic illustration of the *A. mississippiensis* bronchial tree with dorsobronchus 5 (the
1053 fourth dorsobronchus) highlighted in blue, and the laterobronchi highlighted in magenta. (E)
1054 Diagrammatic illustration of the bronchial tree of *S. camelus* with dorsobronchus 4 highlighted
1055 in blue, and the laterobronchi highlighted in magenta. Ostriches = magenta circles. Alligators =
1056 blue triangles.
1057
1058 **Figure 22. Ratio of the distances from the carina to the major secondary bronchi and total**
1059 **distance from the carina to D5 in *A. mississippiensis* and D4 in *S. camelus*.** Top: The relative
1060 distances from the carina to the cervical ventral bronchus and then to each consecutive
1061 dorsobronchus (2-5) in *A. mississippiensis*. Bottom: The relative distances from the carina to the
1062 first ventrobronchus and then each consecutive dorsobronchus (1-4) in *S. camelus*. The colors
1063 follow the hypotheses of homology. There is limited intraspecific variation in all measures
1064 suggesting that the relative distances of secondary bronchi from the carina are strongly
1065 ontogenetically conserved. Further, the only substantial difference between the two taxa is the
1066 distance from the carina to D2/D1 suggesting the other distances may be conserved within
1067 Archosauria.
1068
1069 **Figure 23. Schematic of hypotheses of pulmonary homology shared between the developing**
1070 **chick lung (A) and the adult alligator lung (B).** A) Diagrammatic image of the embryonic chick
1071 respiratory track at day 8 of development showing the initial emergence of the air sacs from the
1072 bronchial tree, prior to their massive expansion beyond the boundary of the gas exchanging
1073 lung; image redrawn and modified from Sakiyama et al. (Sakiyama et al., 2000). B)
1074 Diagrammatic simplified illustration of the bronchial tree and lung of an adult alligator lung in
1075 left lateral view. Colors denote hypothesized homologous regions. Abbreviations: AAS,
1076 abdominal air sac; CGB, caudal group bronchi; CLS, clavicular air sac; CRTS, cranial thoracic air
1077 sac; CS, cervical air sac; CVB, cervical ventral bronchus; D2, dorsobronchus 2; LB, laterobronchi.
1078 Images not to scale.
1079
1080 **Figure 24. Homology hypotheses for the archosaurian bronchial trees.** Segmented solid
1081 surface models of the bronchial tree of *A. mississippiensis* (A, D, G, I), and *S. camelus* (B, C, E, F,
1082 H, K), all in dorsal view. Colors represent hypothesized homologous primary and secondary
1083 bronchi for the two taxa with the "bronchial homology hypothesis 1" (B, E, H): the ostrich
1084 ventrobronchi are homologous to the alligator cervical ventral bronchus. "Bronchial homology
1085 hypothesis 2" (C, F, K): the avian ventrobronchi are homologous to the alligator medial bronchi,
1086 and ventrobronchi 2-4 are homologous to the alligator medial bronchi; (K) demonstrates the
1087 angle of orientation of the secondary bronchi in both taxa on the dorsal surface of the primary
1088 bronchus. Abbreviations: CVB, cervical ventral bronchus; D, dorsobronchi; M, medial bronchi; V,
1089 ventrobronchi; H1, hypothesis 1; H2, hypothesis 2.
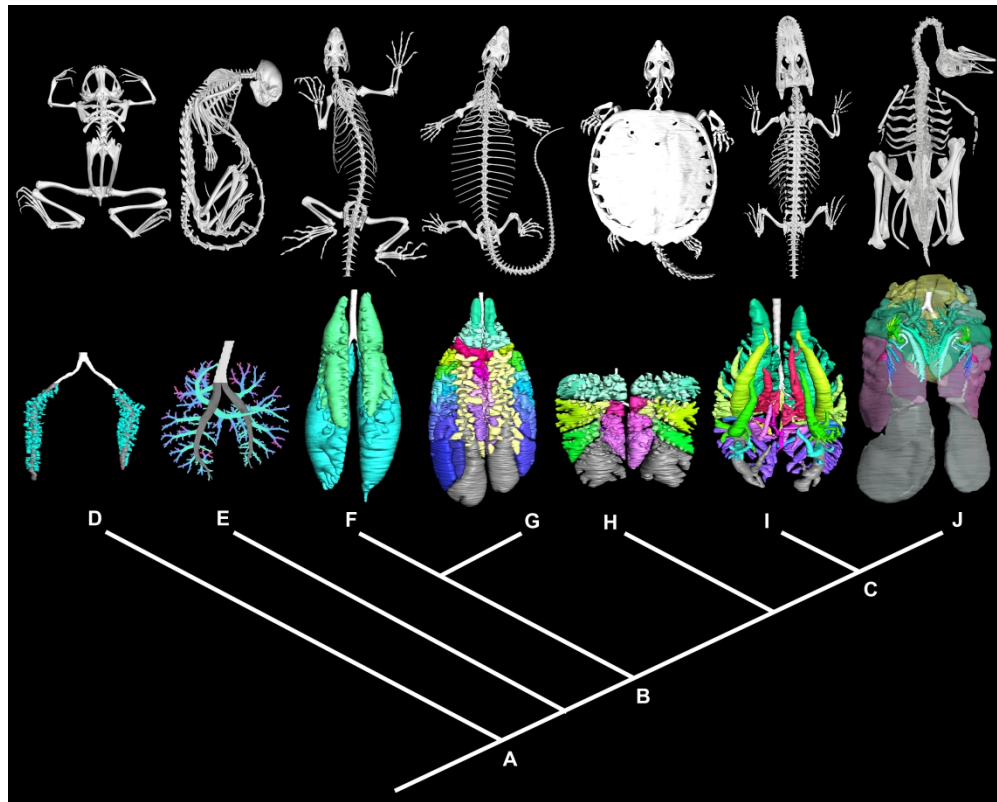
Figure 1. Phylogeny for Tetrapoda demonstrating the structural diversity of the tetrapod lung. A) Amniota; B) Sauropsida; C) Archosauria. Volume rendered skeleton and surface model of the bronchial tree of: D) *Xenopus* sp.; E) *Saguinus* sp., (with a diagrammatic illustration of a standardized primate bronchial tree); F) *Iguana iguana* (modified from Cieri et al., 2014); G) *Varanus exanthematicus* (modified from Schachner et al., 2014); H) *Chelydra serpentina* (modified from Schachner et al., 2017); I) *Alligator mississipiensis*; and, J) *Struthio camelus*. Images not to scale.
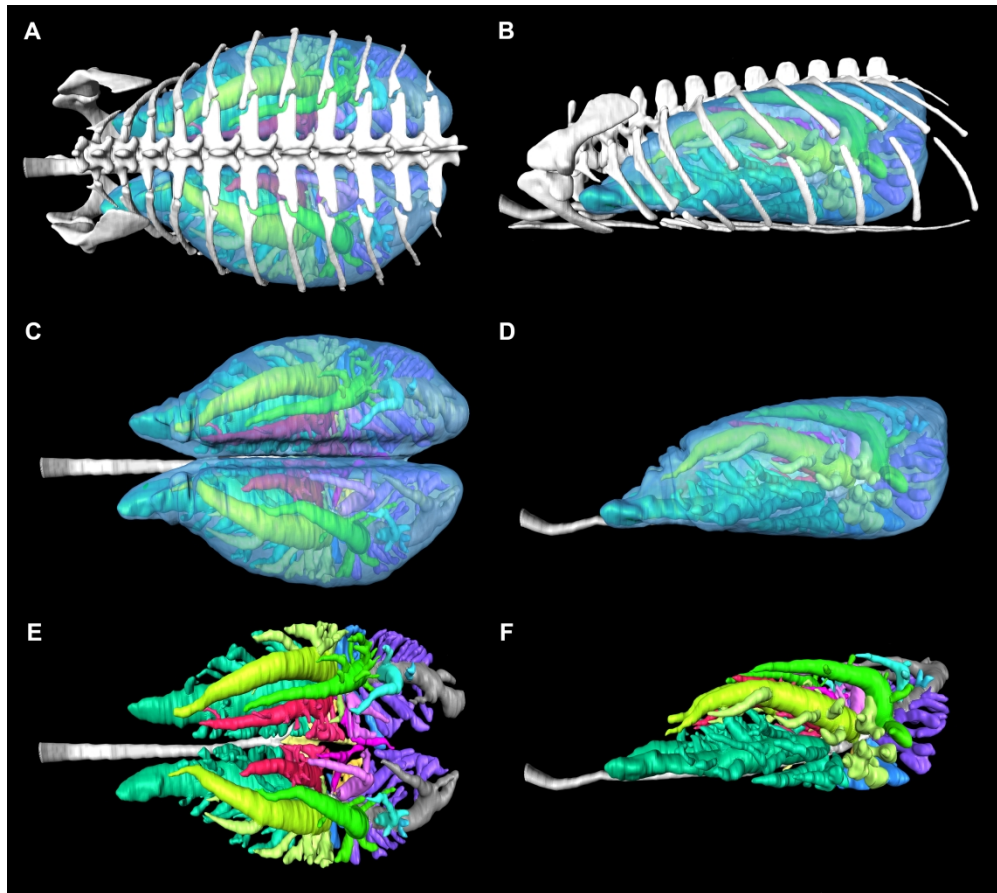
Figure 2. Segmented 3D surface model of the thorax, lung, and bronchial tree of *A. mississippiensis*. *A. mississippiensis* 11 (live) during a natural apnea in dorsal (A, C, E), and left lateral (B, D, F) views. Parabronchi (i.e., connections between the primary, secondary and tertiary bronchi) are not shown.
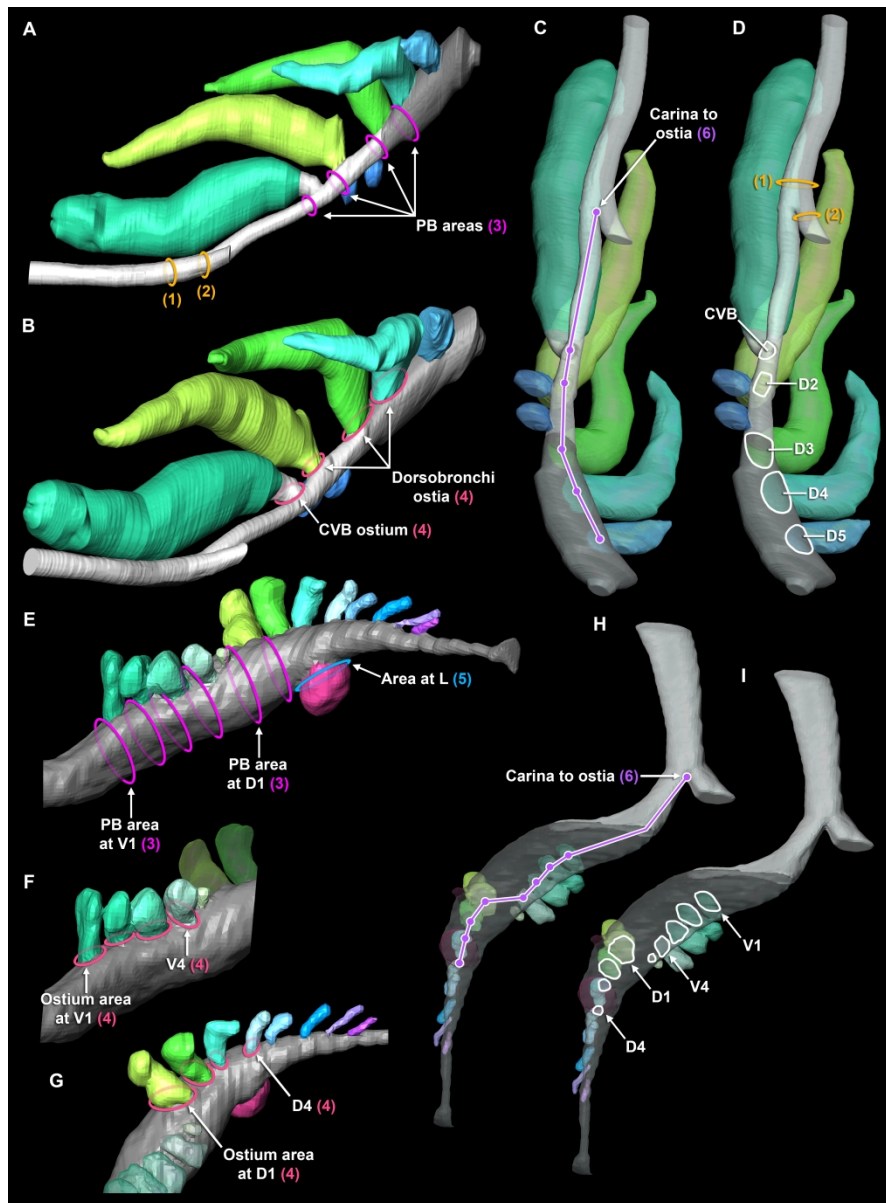
Figure 3. Diagrammatic models demonstrating the quantitative metrics. Simplified and reduced digital model of the bronchial tree of the right lung of *Alligator mississippiensis* in medial (A), craniomedial (B), and ventral (C, D) views, with the tertiary, medial, caudal and lateral bronchi all removed. Simplified and reduced digital model of the bronchial tree of the right lung of *Struthio camelus* in (E, F), dorsomedial (G), and ventral (H, I) views. These models are 3D representations and indications of the 2D quantitative metrics obtained from the DICOM images in OsiriX. A) Gold rings represent the metrics obtained at the trachea (metric 1) and primary bronchus (metric 2) in the alligator. Pink oblique rings demonstrate the sites where metrics were taken for the area of the primary bronchus, perpendicular to the origin of the secondary bronchus (metric 3). B) Red oblique rings represent the site where the metrics were taken for the area of the ostium for each secondary bronchus as it branched from the primary bronchus (metric 4). C-D) Diagram of where metrics were taken for the distances from the carina to each of the large secondary bronchial ostia (metric 6) (C) with the bronchi labeled (D) (metrics 1 and 2 are also labeled in this view). E) Pink oblique circles demonstrating the position of metric 3 in the ostrich. Blue oblique circle demonstrates metric 5 as measured around the large laterobronchus on *S. camelus*. F-G) Red rings demonstrate metric 4 in *S.*

camelus for the ventrobronchi and dorsobronchi. H-I) Diagram of where metrics were taken for the distances from the carina to each of the large secondary bronchial ostia (metric 6) in *S. camelus* with the measurement diagram (H) and the labeled ostia (I). Abbreviations: CA, carina; CVB, cervical ventral bronchus; D2-D5, dorsobronchi 2-5; L, laterobronchus; PB, primary bronchus; V1-4, ventrobronchi 1-4. Numbers indicate specific metrics described in methods. Images not to scale.
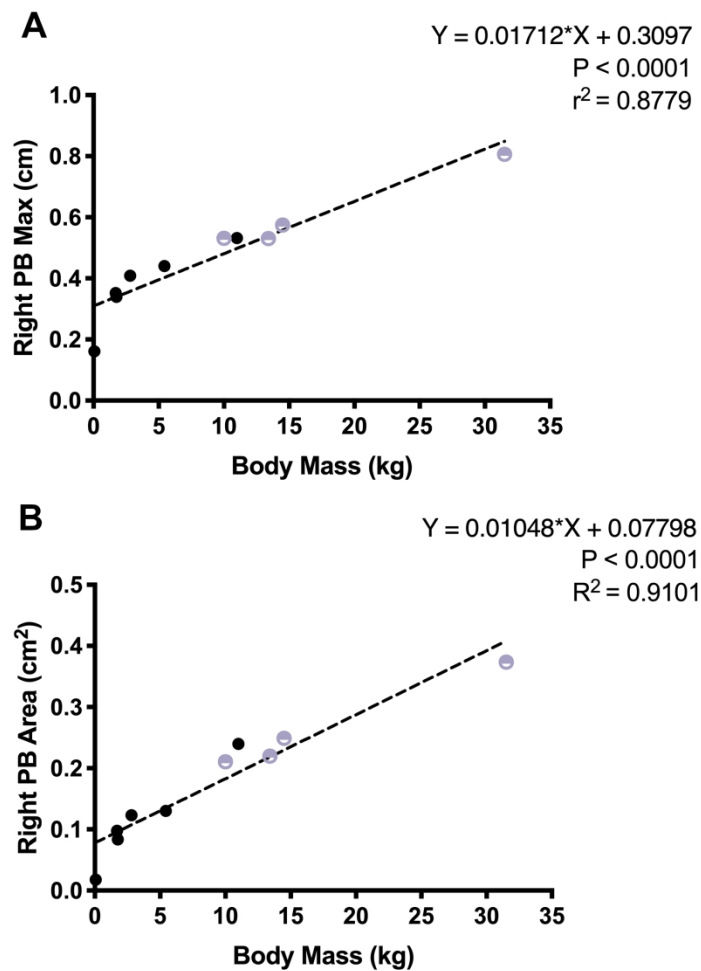
Figure 4. Measured and imputed body masses of *A. mississippiensis* scaled to pulmonary measures across ontogeny. (A) measured/imputed body mass scaled to the maximum diameter of the right primary bronchus just distal to the bifurcation from the trachea; (B) measured/imputed body mass scaled to the area of the right primary bronchus at the same location as (A).
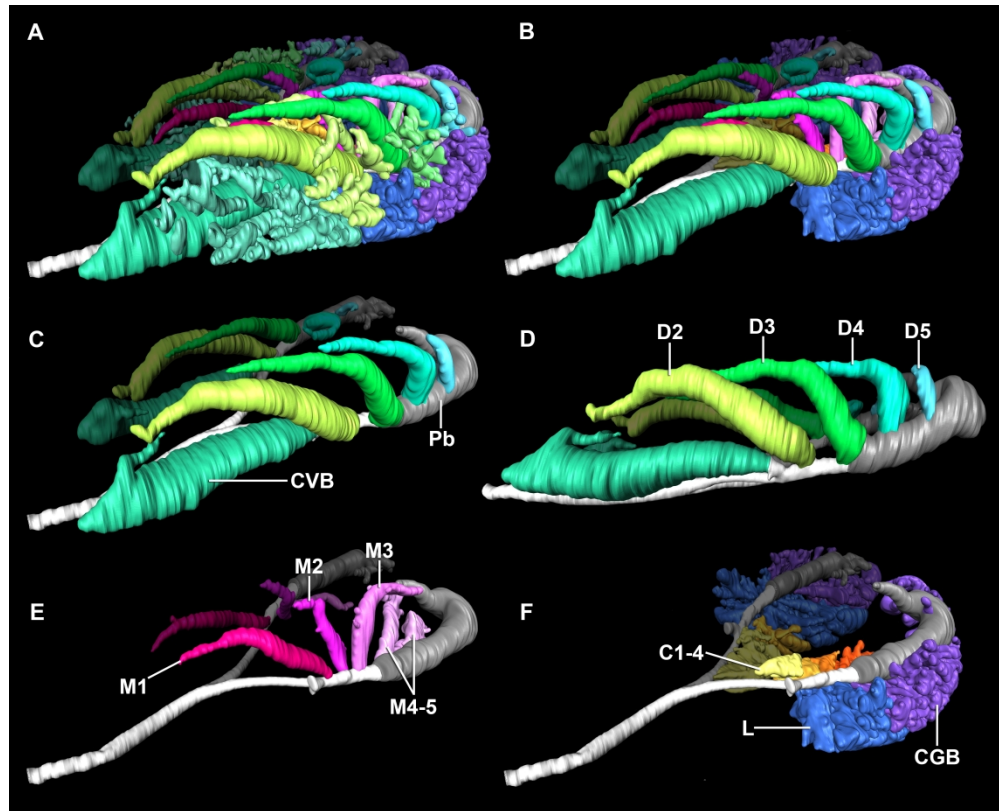
Figure 5. Segmented 3D surface model of the primary, secondary, and large tertiary airways of *A. mississippiensis* 64. Specimen is deceased, artificially inflated, and all images in left craniolateral view (except for D). A) The primary, secondary, and large tertiary bronchi; B) the primary and secondary bronchi (the tertiary bronchi have been removed); C) the primary bronchi, the cervical ventral bronchus, and the dorsobronchi; D) image (C) in left lateral view; E) the primary and medial (M) bronchi; F) the primary bronchi, the laterobronchi, the cardiac lobes, and the caudal group bronchi. Parabronchi (i.e., connections between the primary, secondary and tertiary bronchi) are not shown. Abbreviations = C, cardiac lobes; CGB, caudal group bronchi; CVB, cervical ventral bronchus; D2-5, dorsobronchi 2-5; L, laterobronchi; M1-5, medial bronchi; Pb, primary bronchus.
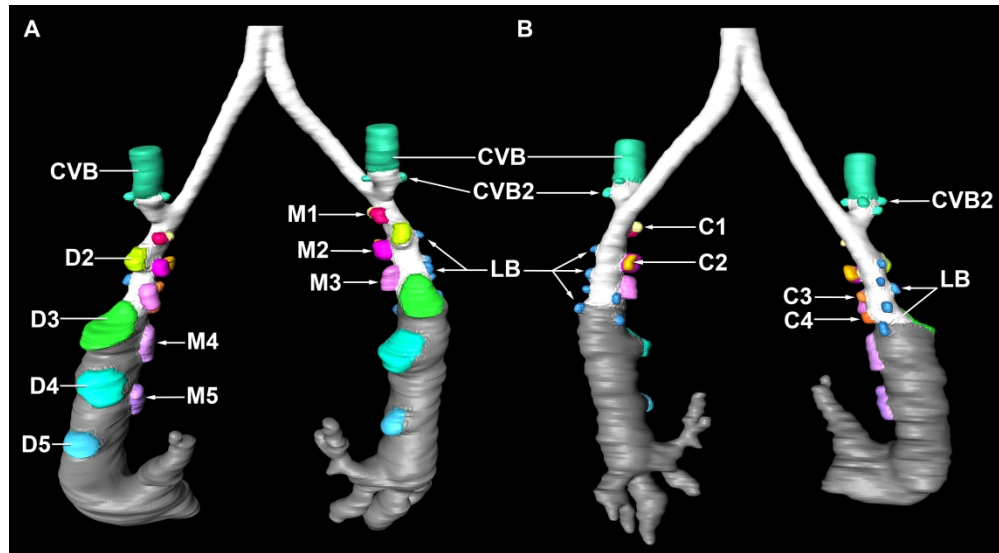
Figure 6. Segmented 3D surface model of the bronchial tree of *A. mississippiensis* 64. Bronchial tree in dorsal (A) and ventral (B) views, with the ostia of the major secondary and a few tertiary branches represented as stumps to visually demonstrate clear branching pattern. Abbreviations: C1-4, cardiac lobes 1-4; CVB, cervical ventral bronchus; CVB2, secondary branches off of the cervical ventral bronchus; D2-5, dorsobronchi 2-5; LB, laterobronchi; M1-5, medial bronchi 1-5.
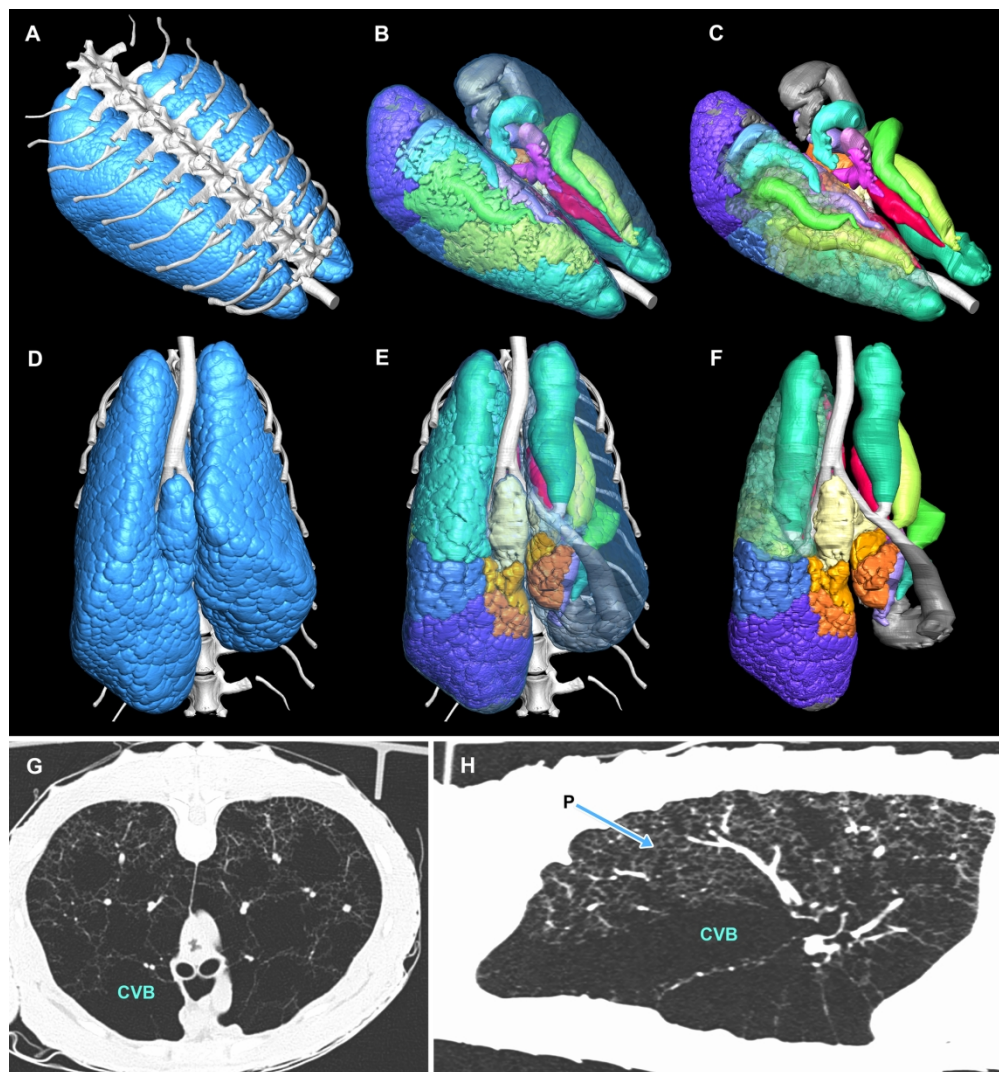
Figure 7. Segmented 3D surface model of the dorsal vertebrae and ribs, lung surface, and bronchial tree of a hatchling *A. mississippiensis* (AM041315-1) and CT images of a live adult ("Stumpy"). Hatchling thorax model in left craniolateral (A-C) and ventral (D-F) views generated from µCT data. Lung surface and axial skeleton are shown in (A), (D), and (E). Surface of the lungs and the tertiary bronchi of the left lung are made semi-translucent in (B-C) and (E-F) to demonstrate the position of the major primary and secondary airways within the lung and relative to the smaller interconnecting branches (=parabronchi). Lung surface and tertiary bronchi are removed from the left lung, and the tertiary are made semi-translucent in (C) and (F) to further demonstrate these relationships. Axial (G) and parasagittal (H) CT images of a live adult *A. mississippiensis* (scanned in a supine position) demonstrating the pulmonary heterogeneity and regional distribution of the parenchyma within the lung. Abbreviations: CVB, cervical ventral bronchus; P, parenchyma.

195x208mm (300 x 300 DPI)
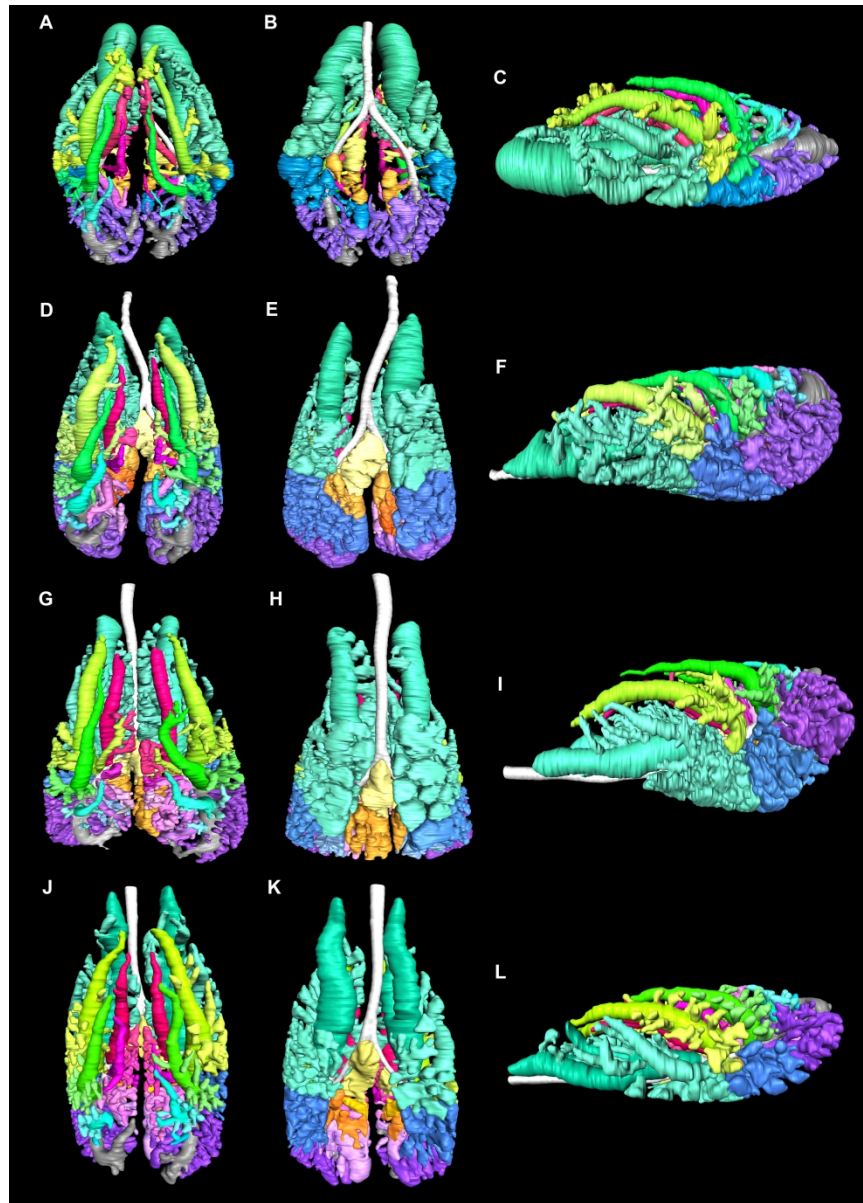
Figure 8. Intraspecific and methodological variation in the bronchial tree of *Alligator mississippiensis*. Segmented 3D surface models of the bronchial tree of four different individuals. Top row: The lungs of alligator 81 (deceased), shown in dorsal (A), ventral (B), and left lateral (C) views, were completely dissected out of the thorax, and inflated via a syringe prior to scanning. Second row: alligator 64 (deceased), shown in dorsal (D), ventral (E), and left lateral (F) views, was inflated via a syringe, and scanned in situ in the torso. Third row: "Stumpy," shown in dorsal (G), ventral (H), and left lateral (I) views, was scanned live, unsedated, and in an upside down (supine) position. Bottom row: alligator 15, shown in dorsal (J), ventral (K), and left lateral (L) views, was scanned live, unsedated, and prone position. Images not to scale.
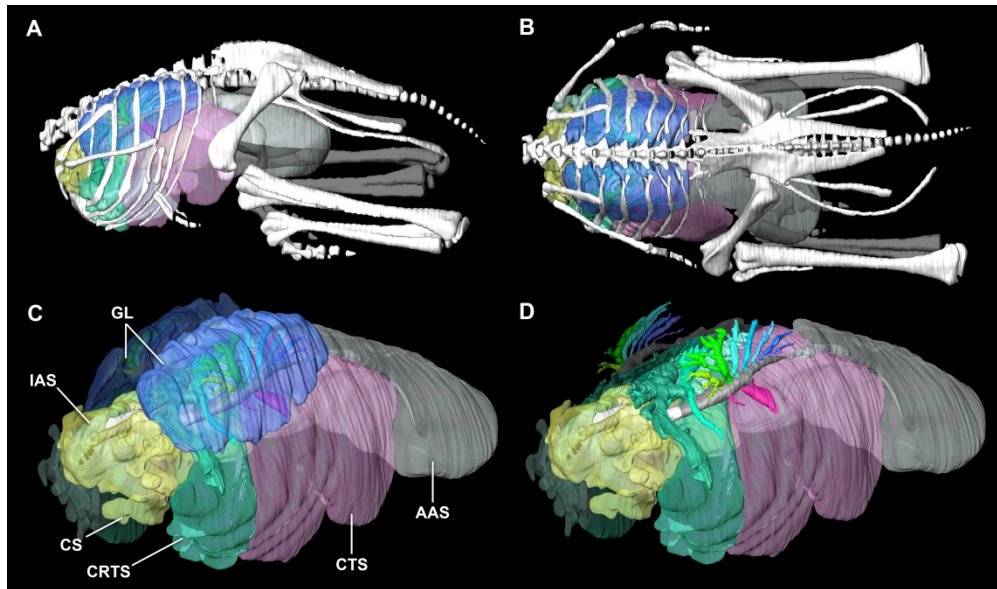
Figure 9. Segmented 3D surface model of the postcranial skeleton and respiratory system of *Struthio camelus* 6 (deceased, artificially inflated). *S. camelus* model in left lateral (A), dorsal (B), and left craniolateral (C-D) views. No secondary pulmonary diverticula are shown. C) Lung surface and air sacs. D) Lung surface has been removed showing a solid representation of the bronchial tree and the direct connections to the extrapulmonary air sacs. Note that the parabronchi are not shown (connections between the dorsobronchi and ventrobronchi) as they are too small to be segmented from the CT data due to resolution of a medical grade scanner. Additionally, the interclavicular and cervical air sacs have been segmented as a single unit due to the inability to differentiate between the boundaries due to the resolution of the scan. Abbreviations: AAS, abdominal air sac; CRTS, cranial thoracic air sac; CS, cervical air sac; CTS, cranial thoracic air sac; GL, gas exchanging lung; IAS, interclavicular air sac.
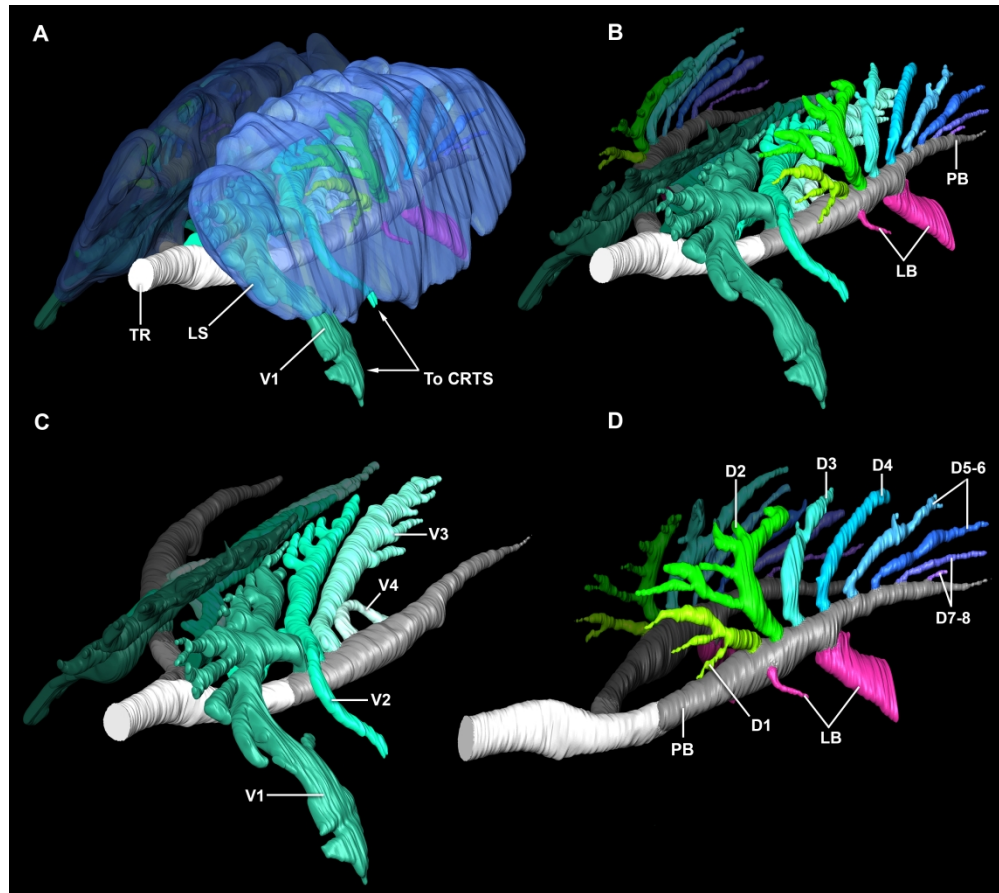
Figure 10. Segmented 3D surface model of the gas exchanging lung and bronchial tree of *S. camelus* 6. Model is shown in left craniolateral (A-C) and left lateral (D) views. The surface of the gas exchanging lung is represented as semi-translucent blue and the negative space within the bronchial tree is shown as solid. Note that the parabronchi are not shown (connections between the dorsobronchi and ventrobronchi) as they are too small to be segmented from the CT data due to resolution of a medical grade scanner. Abbreviations: CRTS, cranial thoracic air sac; D1-8, dorsobronchi 1-8; LB, laterobronchi; LS, lung surface; PB, primary bronchus; TR, trachea; V1-4, ventrobronchi 1-4.
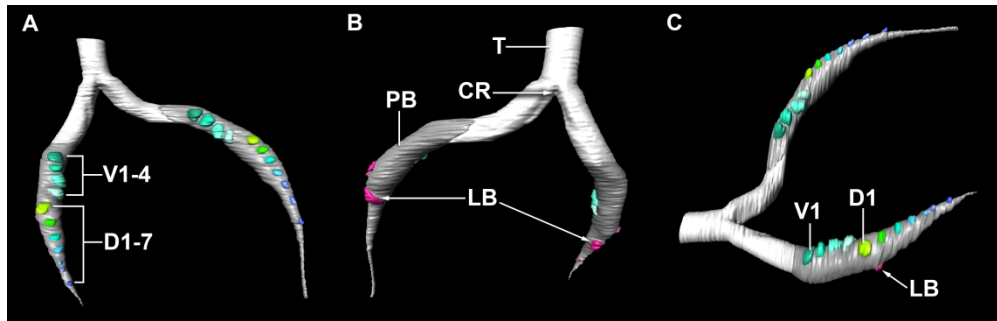
Figure 11. Segmented 3D surface model of the bronchial tree of *S. camelus* 6. Model is shown in dorsal (A), ventral (B), and left dorsolateral (C) views, with the ostia of the major secondary branches represented as stumps to visually demonstrate clear branching patterns. Abbreviations: CR, carina; D1-7, dorsobronchi 1-7; LB, laterobronchi; PB, primary bronchus; T, trachea; V1-4, ventrobronchi 1-4.
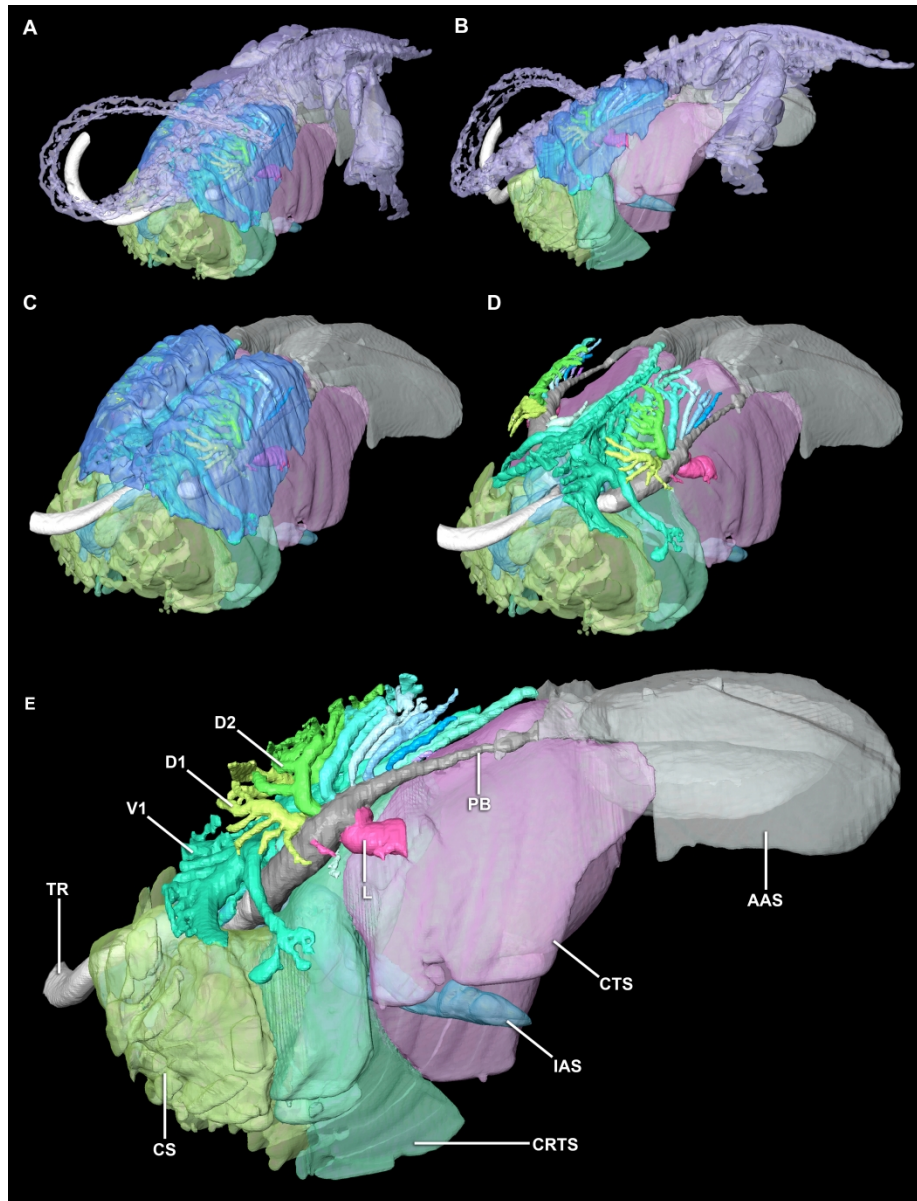
Figure 12. Segmented 3D surface model of the entire respiratory system of *S. camelus* 7. Model is shown in left craniolateral (A, C, D) and lateral views (B, E). The pulmonary diverticula are visible in (A) and (B) and can be clearly seen extending cranially and caudally to the gas-exchanging lung, as well as positioned dorsally to the ventilatory air sacs. The pulmonary diverticula are removed in (C-E) and demonstrate the lack of continuity with the air sacs. Abbreviations: AAS, abdominal air sac; CS, cervical air sac; CRTS, cranial thoracic air sac; CTS, caudal thoracic air sac; D1-2, dorsobronchi 1-2; IAS, interclavicular air sac; L, laterobronchus; PB, primary bronchus; TR, trachea; V1, ventrobronchus 1. Images not to scale.
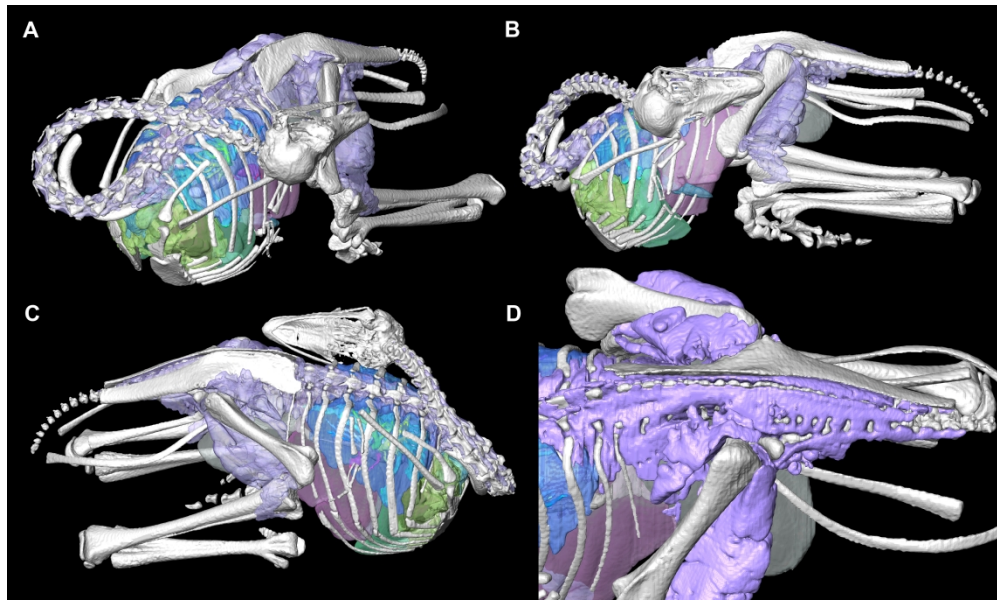
Figure 13. Segmented 3D surface model of the skeleton and respiratory system of *S. camelus* 7. Model is shown in left craniolateral (A), left lateral (B), right lateral (C), and left dorsolateral views with the left ilium removed (D). The pulmonary diverticula are visualized as a solid in (D) to clarify the relationships between these structures and the adjacent skeletal tissues.
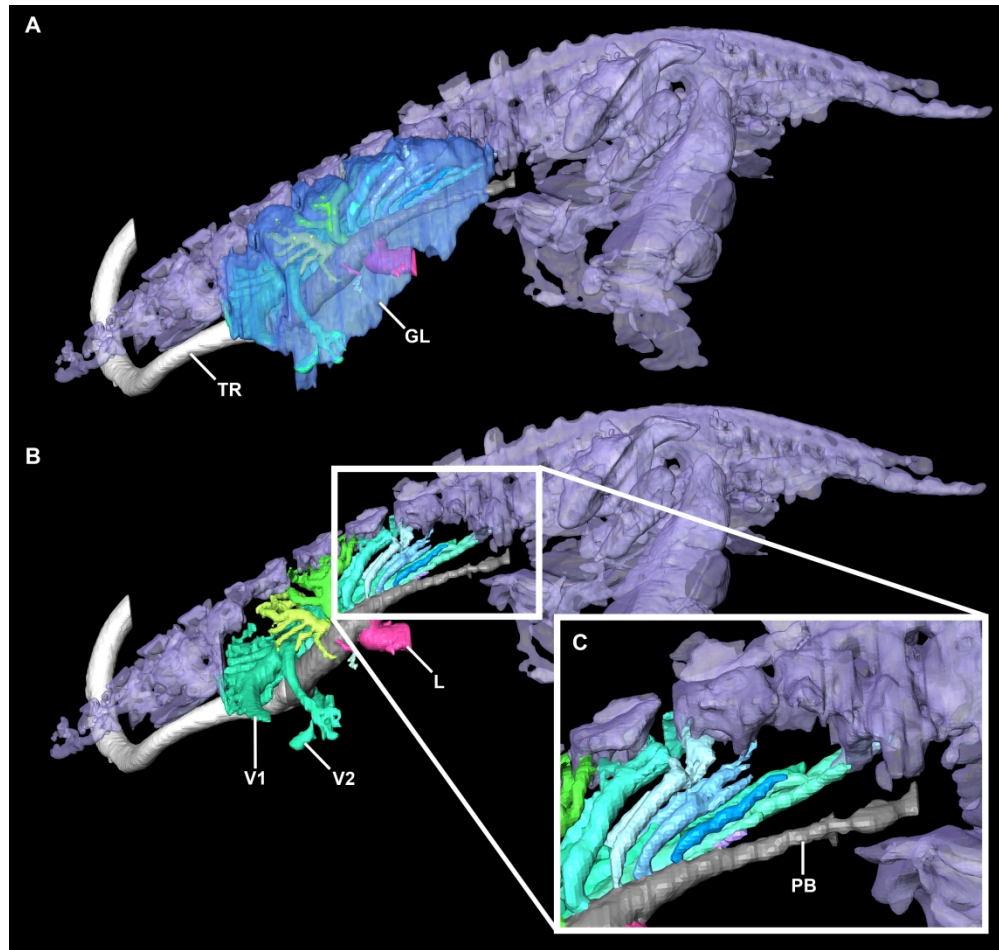
Figure 14. Segmented 3D surface model of the gas-exchanging lung, bronchial tree, and pulmonary diverticula of *S. camelus* 7. Model is shown in left lateral view, demonstrating the origin of the majority of the diverticula from the secondary airways, and directly from the surface of the lung, but distinct from the caudal extent of the primary bronchus as it extends beyond the gas-exchanging lung to balloon into the abdominal air sac. Abbreviations: GL, gas exchanging lung; L, laterobronchus; PB, primary bronchus; TR, trachea; V1-2, ventrobronchi 1-2.
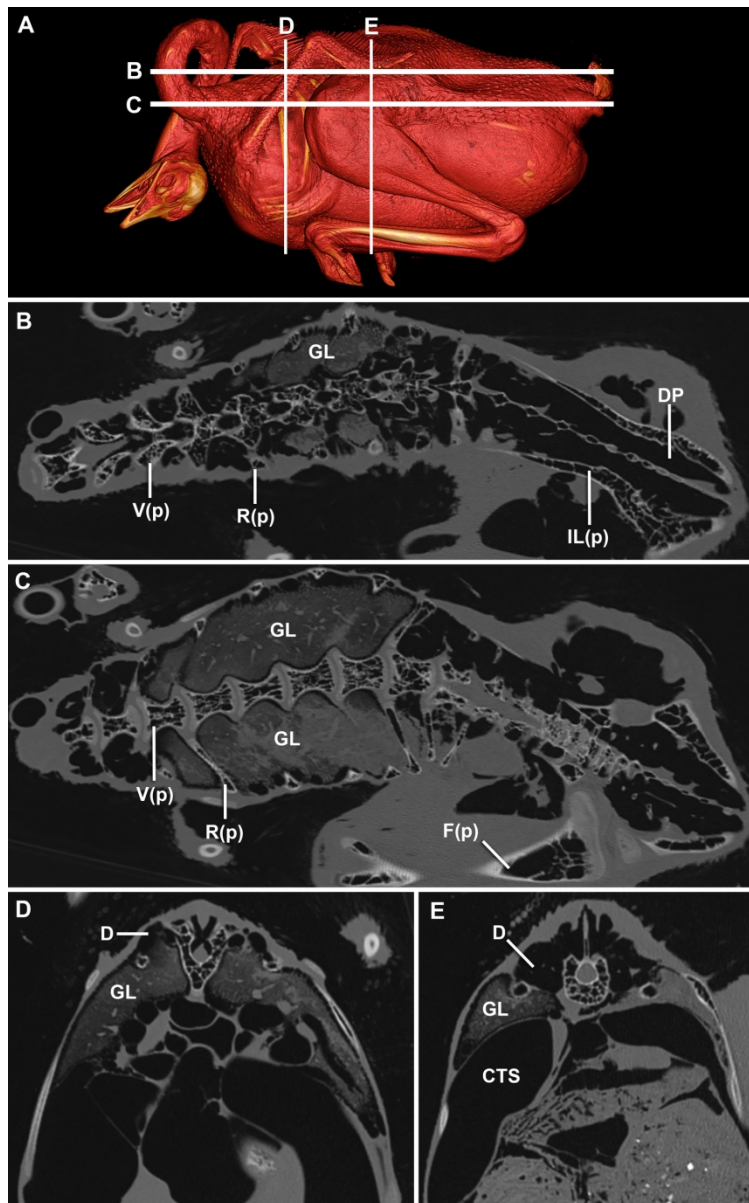
Figure 15. Volume rendered model and coronal CT slices of *S. camelus* 10 demonstrating extensive axial and appendicular postcranial pneumaticity. (A) Volume rendered 3D model of a juvenile S. camelus in left lateral view with lines demonstrating the location of the two coronal DICOM slices shown at positions (B) and (C), and two axial slices shown at positions (D) and (E). Abbreviations: D, diverticula; DP, diverticula pelvica; F(p), femur (pneumatized); GL, gas-exchanging lung; R(p), rib (pneumatized); V(p), vertebra (pneumatized).

137x219mm (300 x 300 DPI)
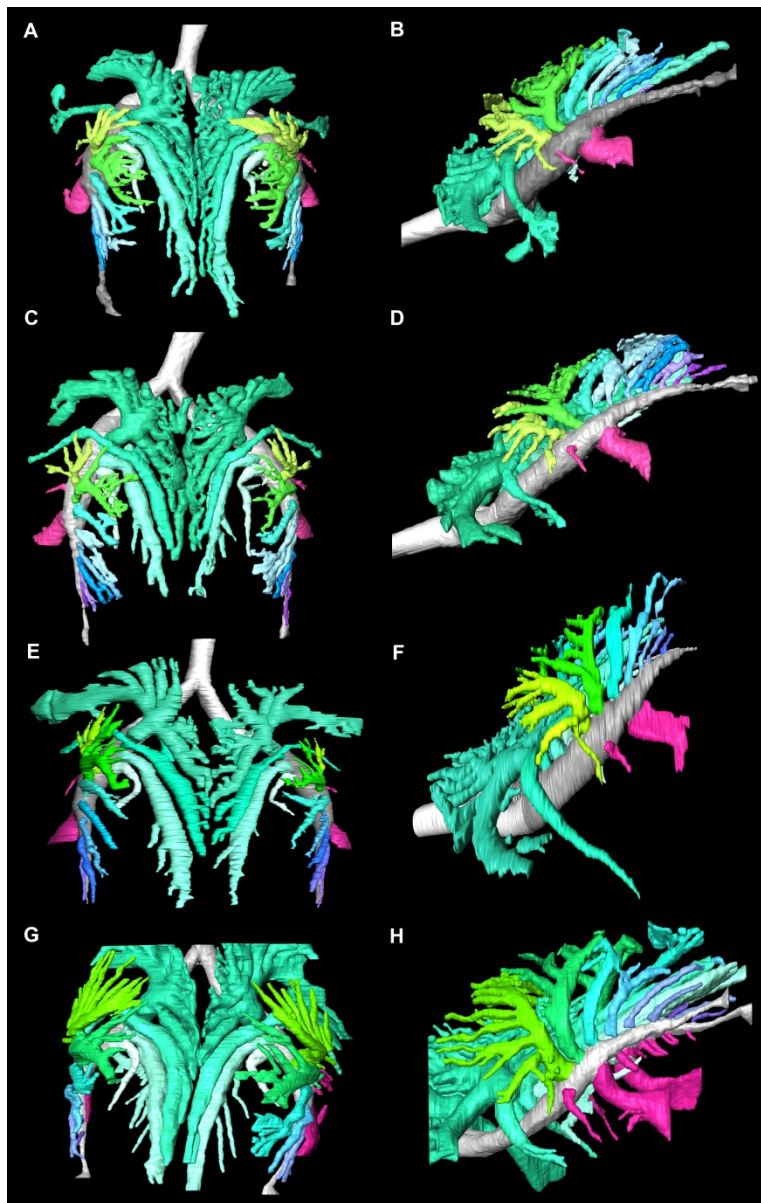
Figure 16. Intraspecific variation in the bronchial tree of *Struthio camelus*. Segmented 3D surface models of *S. camelus* 7 in dorsal (A) and left lateral (B) views, *S. camelus* 8 in dorsal (C) and left lateral (D) views, *S. camelus* 10 in dorsal (E) and left lateral (F) views, and *S. camelus* 11 in dorsal (G) and left lateral (H) views. Images not to scale.
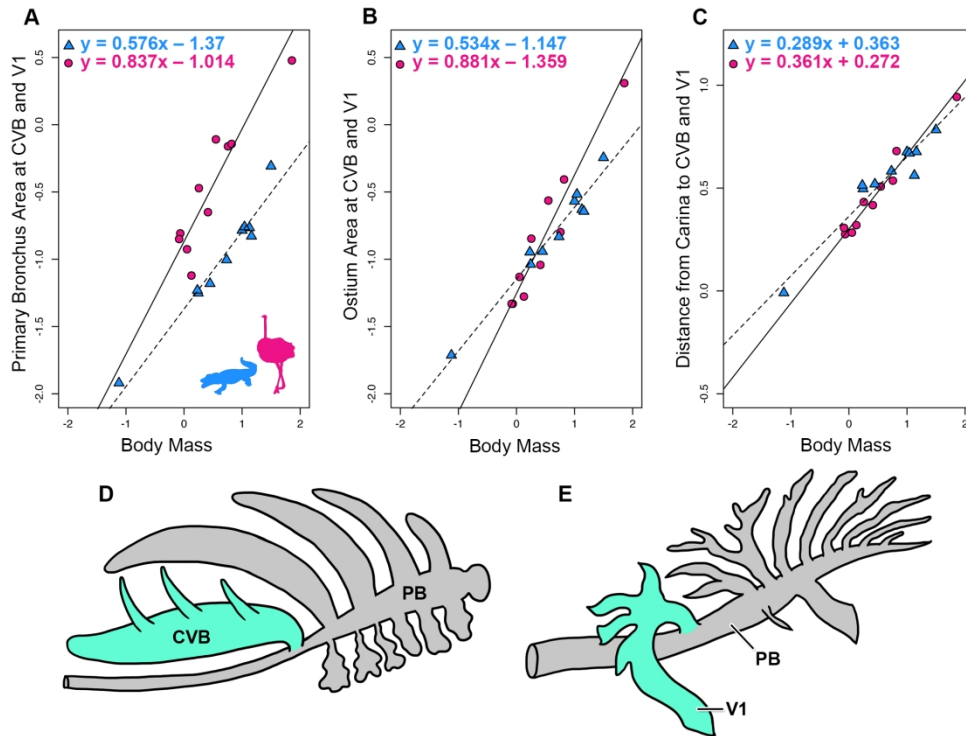
Figure 17. Standard major axis regressions of the log of body mass and the log of the following anatomical measurements: (A) Cross sectional area of intrapulmonary primary bronchus at the level of CVB (alligator) and V1 (ostrich), (B) cross sectional area of ostium of CVB and V1 (C) distance from the carina to the ostium of the CVB and V1. (D) Diagrammatic illustration of the *A. mississippiensis* bronchial tree with the cervical ventral bronchus highlighted in green. (E) Diagrammatic illustration of the bronchial tree of *S. camelus* with the cervical ventral bronchus highlighted in green. Abbreviations: CVB, cervical ventral bronchus; PB, primary bronchus; V1, ventrobronchus. Ostriches = magenta circles. Alligators = blue triangles.
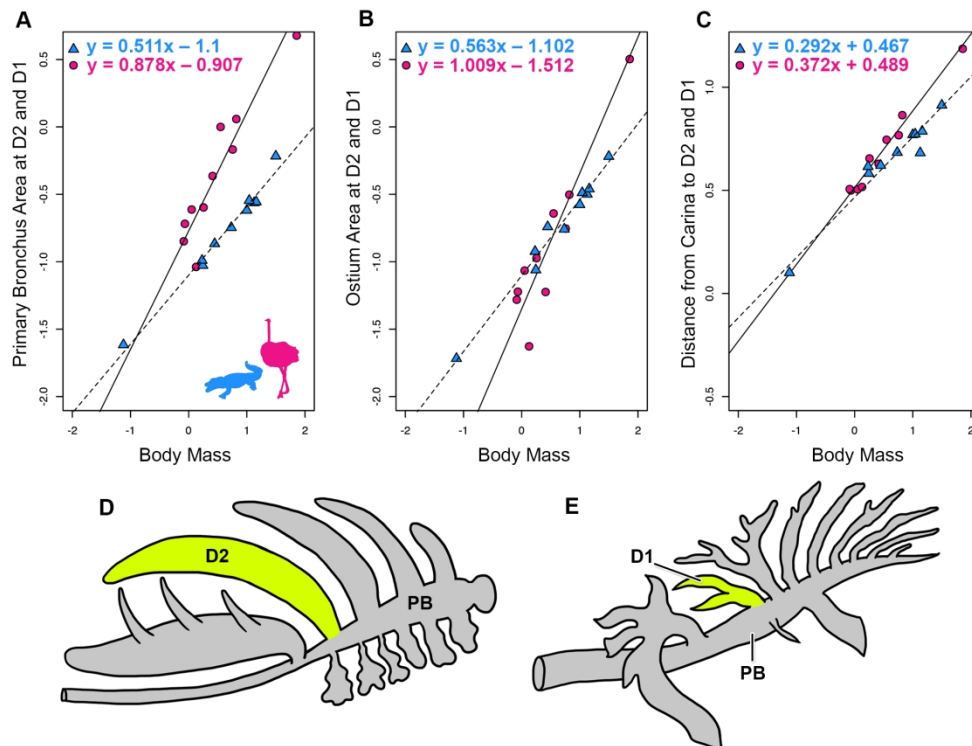
Figure 18. Standard major axis regressions of the log of body mass and the log of the following anatomical measurements. (A) Cross sectional area of intrapulmonary primary bronchus at the level of D2 (*Alligator*) and D1 (*Struthio*) and body mass (B) cross sectional area of ostium of the D2 and D1 (C) distance from the carina to the ostium of D2 and D1 (D) Diagrammatic illustration of the *A. mississippiensis* bronchial tree with dorsobronchus 2 (the first dorsobronchus) highlighted in lime. (E) Diagrammatic illustration of the bronchial tree of *S. camelus* with dorsobronchus 1 highlighted in lime. Ostriches = magenta circles. Alligators = blue triangles.
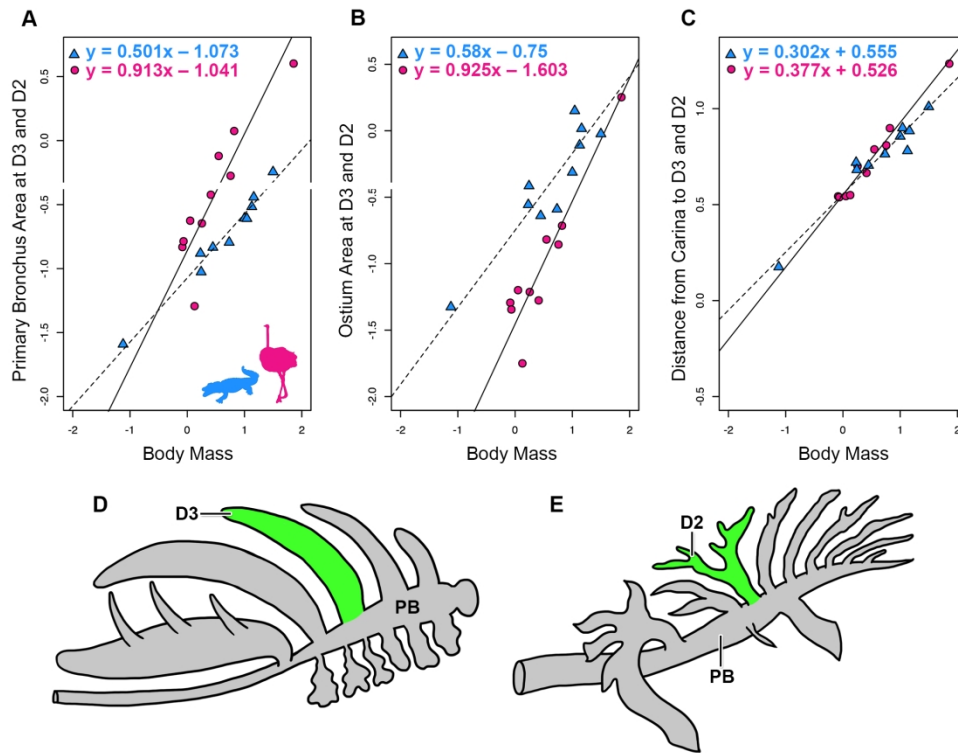
Figure 19. Standard major axis regressions of the log of body mass and the log of the following anatomical measurements: (A) Cross sectional area of intrapulmonary primary bronchus at the level of D3 (*Alligator*) and D2 (*Struthio*) and body mass (B) cross sectional area of ostium of the D3 and D2 (C) distance from the carina to the ostium of D3 and D2 (D) Diagrammatic illustration of the *A. mississippiensis* bronchial tree with dorsobronchus 3 (the second dorsobronchus) highlighted in neon green. (E) Diagrammatic illustration of the bronchial tree of *S. camelus* with dorsobronchus 2 highlighted in neon green. Ostriches = magenta circles. Alligators = blue triangles.
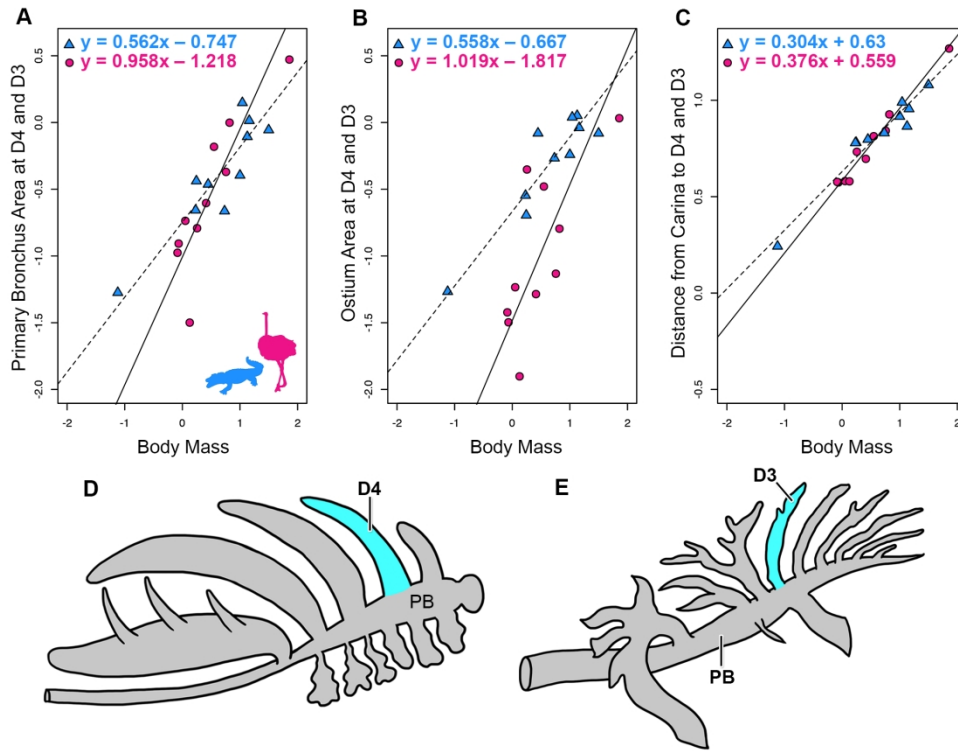
Figure 20. Standard major axis regressions of the log of body mass and the log of the following anatomical measurements: (A) Cross sectional area of intrapulmonary primary bronchus at the level of D4 (*Alligator*) and D3 (*Struthio*) and body mass (B) cross sectional area of ostium of the D4 and D3 (C) distance from the carina to the ostium of D4 and D3 (D) Diagrammatic illustration of the *A. mississippiensis* bronchial tree with dorsobronchus 4 (the third dorsobronchus) highlighted in aqua. (E) Diagrammatic illustration of the bronchial tree of *S. camelus* with dorsobronchus 3 highlighted in aqua. Ostriches = magenta circles. Alligators = blue triangles.
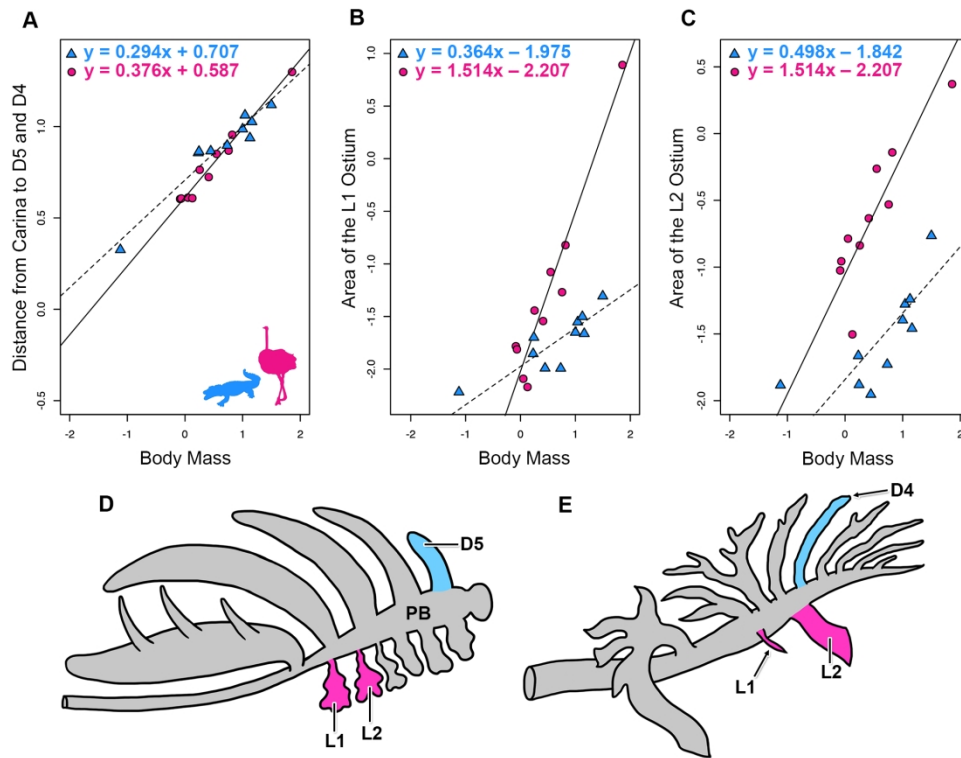
Figure 21. Standard major axis regressions of the log of body mass and the log of the following anatomical measurements: (A) Cross sectional area of intrapulmonary primary bronchus at the level of D5 (*Alligator*) and D4 (*Struthio*) and body mass (B) cross sectional area of the ostium of laterobronchus 1 (C) cross sectional area of the ostium of laterobronchus 2 (D) Diagrammatic illustration of the *A. mississippiensis* bronchial tree with dorsobronchus 5 (the fourth dorsobronchus) highlighted in blue, and the laterobronchi highlighted in magenta. (E) Diagrammatic illustration of the bronchial tree of *S. camelus* with dorsobronchus 4 highlighted in blue, and the laterobronchi highlighted in magenta. Ostriches = magenta circles. Alligators = blue triangles.
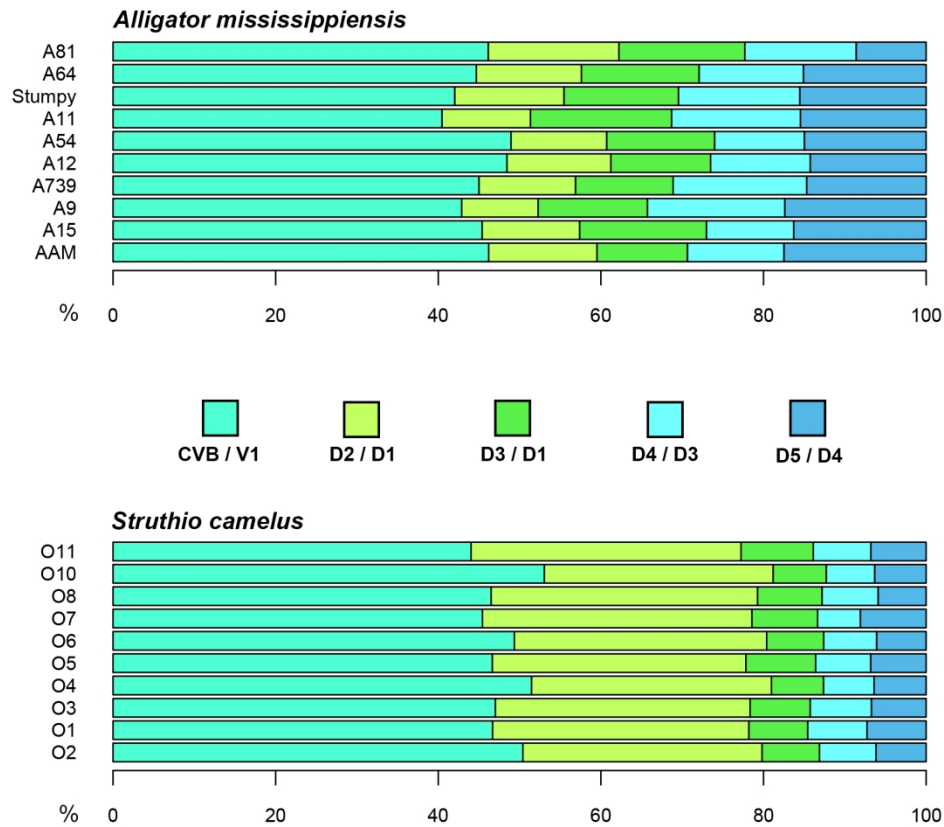
Figure 22. Ratio of the distances from the carina to the major secondary bronchi and total distance from the carina to D5 in *A. mississippiensis* and D4 in *S. camelus*. Top: The relative distances from the carina to the cervical ventral bronchus and then to each consecutive dorsobronchus (2-5) in *A. mississippiensis*. Bottom: The relative distances from the carina to the first ventrobronchus and then each consecutive dorsobronchus (1-4) in *S. camelus*. The colors follow the hypotheses of homology. There is limited intraspecific variation in all measures suggesting that the relative distances of secondary bronchi from the carina are strongly ontogenetically conserved. Further, the only substantial difference between the two taxa is the distance from the carina to D2/D1 suggesting the other distances may be conserved within Archosauria.
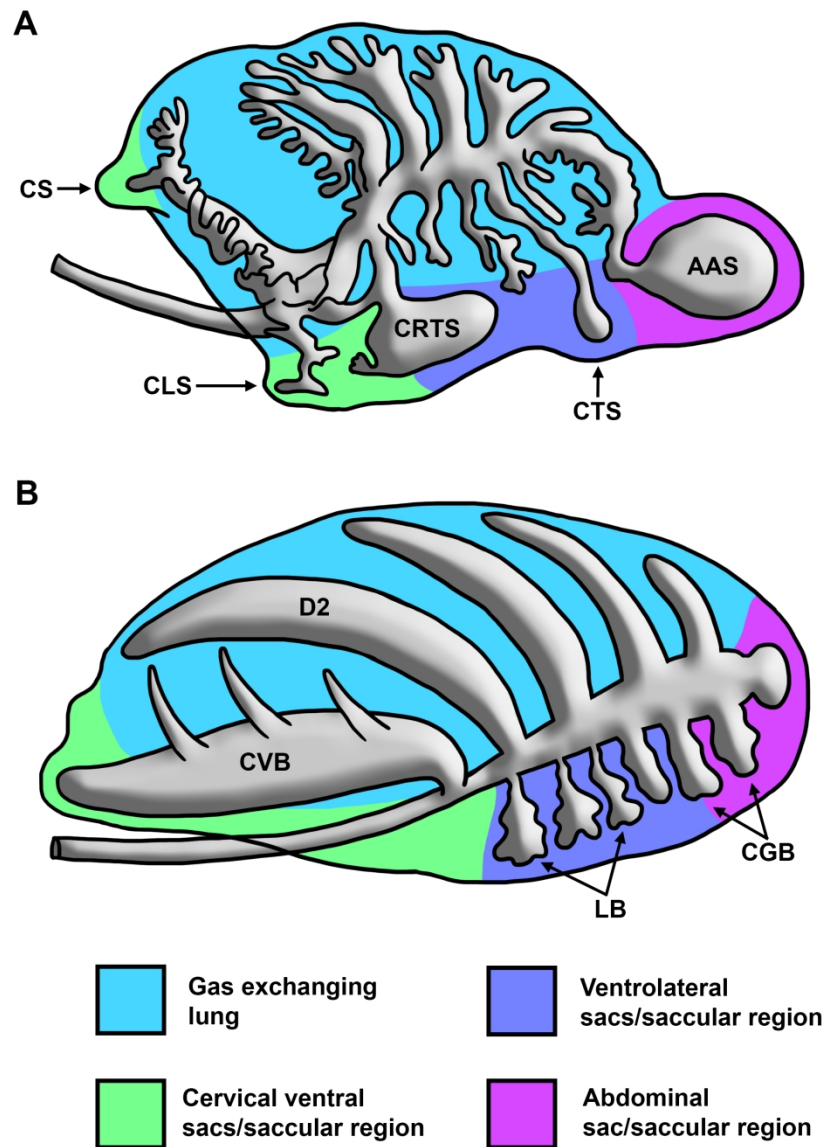
Figure 23. Schematic of hypotheses of pulmonary homology shared between the developing chick lung (A) and the adult alligator lung (B). A) Diagrammatic image of the embryonic chick respiratory track at day 8 of development showing the initial emergence of the air sacs from the bronchial tree, prior to their massive expansion beyond the boundary of the gas exchanging lung; image redrawn and modified from Sakiyama et al. (2000). B) Diagrammatic simplified illustration of the bronchial tree and lung of an adult alligator lung in left lateral view. Colors denote hypothesized homologous regions. Abbreviations: AAS, abdominal air sac; CGB, caudal group bronchi; CLS, clavicular air sac; CRTS, cranial thoracic air sac; CS, cervical air sac; CVB, cervical ventral bronchus; D2, dorsobronchus 2; LB, laterobronchi. Images not to scale.
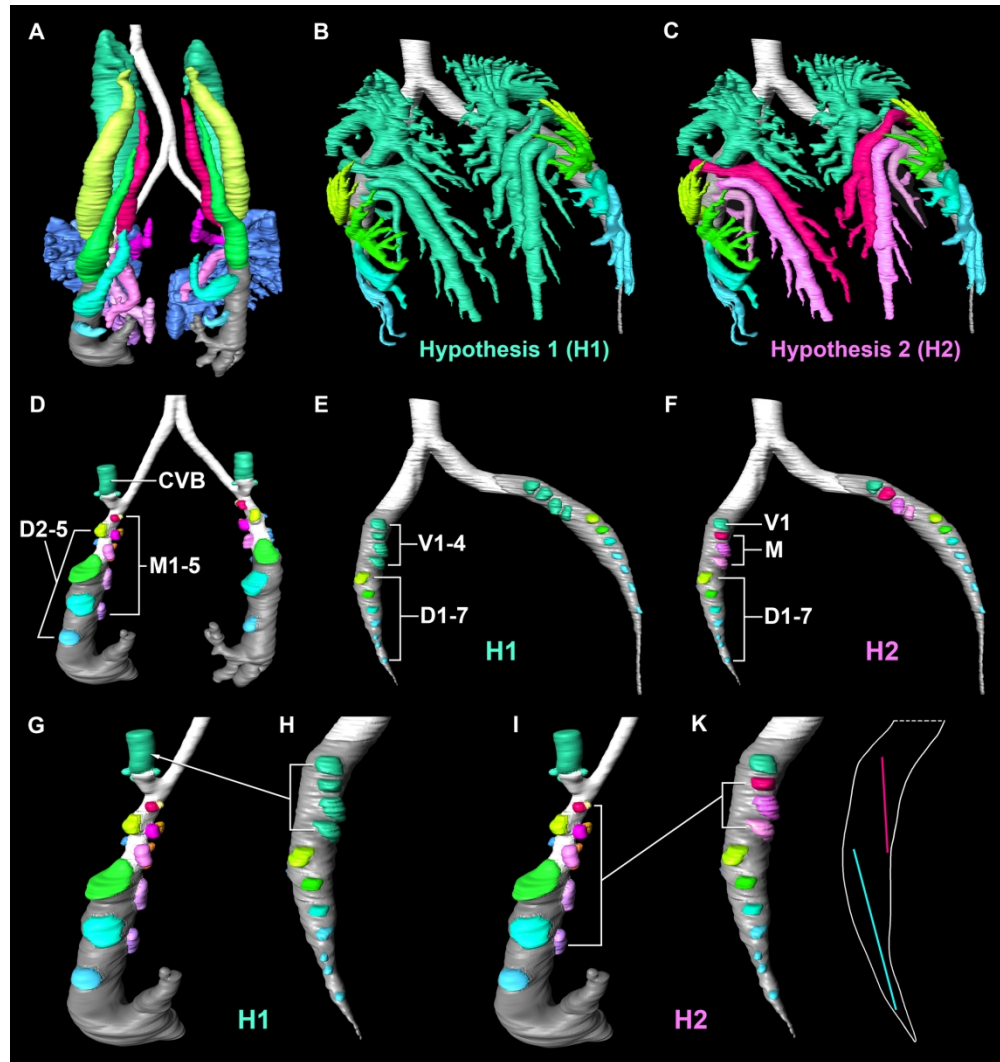
Figure 24. Homology hypotheses for the archosaurian bronchial trees. Segmented solid surface models of the bronchial tree of *A. mississippiensis* (A, D, G, I), and *S. camelus* (B, C, E, F, H, K), all in dorsal view. Colors represent hypothesized homologous primary and secondary bronchi for the two taxa with the "bronchial homology hypothesis 1" (B, E, H): the ostrich ventrobronchi are homologous to the alligator cervical ventral bronchus. "Bronchial homology hypothesis 2" (C, F, K): the avian ventrobronchi are homologous to the alligator medial bronchi, and ventrobronchi 2-4 are homologous to the alligator medial bronchi; (K) demonstrates the angle of orientation of the secondary bronchi in both taxa on the dorsal surface of the primary bronchus. Abbreviations: CVB, cervical ventral bronchus; D, dorsobronchi; M, medial bronchi; V, ventrobronchi; H1, hypothesis 1; H2, hypothesis 2.

187x198mm (300 x 300 DPI)